Replications and Valuations of Contracts on Risk-Neutral Moments

Proposed by Eric Rahal

Under the supervision of Geneviève Gauthier

A thesis presented for the partial fulfilment for the requirement of the degree of
Master of Science (M.Sc) in Financial Engineering

HEC MONTRÉAL

Departement of Decision Sciences
April 2024

Résumé

Les produits dérivés axés sur la volatilité figurent parmi les principaux instruments de gestion des risques offerts par l'ingénierie financière. Ce mémoire vise à répondre à la problématique de la réplication et de l'évaluation de ce type de produit. Nous présentons des stratégies de réplication pour un produit dérivé dont le sous-jacent est la variation quadtratique de l'indice S&P 500. La stratégie de couverture se divise en deux étapes distinctes. Tout d'abord, il y a une réplication statique avec un portefeuille d'options d'achat et de vente, puis une composante dynamique sur le marché des contrats à terme. Nous explorons divers horizons (1 mois, 3 mois, 6 mois et 1 an).

Nous commençons par tester ces stratégies dans un environnement simulé, puis nous les appliquons aux données réelles. Nous constatons une performance globale satisfaisante de la réplication. Cependant, des écarts extrêmes se manifestent pour certains jours. Nous procédons alors à une analyse statistique des erreurs relatives de réplication à l'aide de régressions linéaires. Notre analyse révèle que ces écarts peuvent être expliqués par deux facteurs principaux. Premièrement, une erreur de troncature par rapport aux limites de l'intégrale numérique lors de l'évaluation du portefeuille statique d'options. Deuxièmement, une meilleure performance de la réplication pendant les périodes de crise caractérisées par une combinaison de chocs négatifs sur le sous-jacent et une augmentation de la volatilité implicite pour les options à parité (at-the-money) de 30 jours.

Nous identifions également que ces mêmes facteurs influent lors de l'évaluation de ce contrat. Ainsi, nous suggérons l'utilisation d'un modèle paramétrique qui nous permet d'évaluer le contrat par extrapolation tout en restant cohérent avec la surface de volatilité risque-neutre. Enfin, nous étendons l'utilisation de cette estimation paramétrique à un deuxième contrat portant sur les événements extrêmes négatifs.

Mots-clés: volatilité; couverture de produits dérivés; évènements extrêmes; variation quadratique; gestion des risques; discontinuités

Abstract

Derivatives focused on volatility are among the key risk management instruments provided by financial engineering. This thesis aims to address the challenge of replicating and evaluating such products. We present replication strategies for a derivative with an underlying futures contract on the S&P 500 index. Its payoff approximates the quadratic variation of the index. The replication strategy comprises two distinct steps. Initially, there is a static replication involving a portfolio of call and put options, followed by a dynamic component in the futures market. Various horizons (1 month, 3 months, 6 months, and 1 year) are explored.

We begin by testing these strategies in a simulated environment and then apply them to real data. We observe an overall satisfactory performance in replication. However, extreme deviations occur on certain days. We then proceed with a statistical analysis of the relative replication errors using linear regressions. Our analysis reveals that these deviations can be explained by two main factors. Firstly, there is a truncation error concerning the limits of the numerical integral when evaluating the static options portfolio. Secondly, there is an higher replication performance during crisis periods characterized by a combination of negative shocks to the underlying asset and an increase in the 30-day at-the-money implied volatility.

We also identify that these same factors influence the valuation of this contract. Therefore, we suggest using a parametric model that allows us to assess the contract through extrapolation while remaining consistent with the risk-neutral volatility surface. Finally, we extend the use of this parametric estimation to a second contract related to extreme negative events.

Keywords: volatility; derivatives replication; option market; extreme events; quadratic variation; jump diffusion; volatility trading; risk management

Remerciement

En premier lieu, je voudrais remercier ma directrice Geneviève Gauthier pour sa disponibilité et ses conseils tout le long de ma rédaction. Son talent de pédagogue et sa connaissance aiguisée en finance mathématique ont été primordiaux pour la réalisation de ce mémoire. Je veux également remercier le Professeur David Ardia pour sa disponibilité et nos nombreuses discussions tout le long de ma scolarité de deuxième cycle. Finalement, un remerciement distingué aux membres du jury qui ont accepté de lire et d'évaluer le présent mémoire.

Je veux également remercier mon mentor Nassim Nicholas Taleb pour m'avoir fait découvrir ce monde captivant des options et des variations extrêmes qui leur sont affiliées.

De plus, je veux rendre hommage aux géants des probabilités et de la statistique mathématique, qui nous ont transmis les fondamentaux sur lesquels reposent de nombreux outils techniques appliqués à ce monde aléatoire des marchés financiers.

Une mention particulière au regretté Peter Carr (Caruana) qui nous a quittés tragiquement en mars 2022. Il laisse à la postérité de nombreux travaux, notamment la formule Carr Madan, l'un des principaux outils techniques du présent mémoire. Ainsi qu'à Daniel Kahneman, pionnier de l'économie et de la finance comportementale, qui nous a quittés en mars 2024.

Finalement, je veux remercier mes parents, ma famille et mes amis pour leur soutien tout le long de mes études.

Contents

List of Figures

List of Tables

List of Acronyms

ARMSE Average Root Mean Square Error

ATM At-the-money

Bqv Bondarenko's quadratic variation

CBOE Chicago Board Options Exchange

FRED Federal Reserve Economic Data

IV Implied volatility

NYSE New York Stock Exchange

OTC Over-the-counter

OTM Out-of-the-money

RRMSE Relative Root Mean Square Error

RSE Residual Standard Error

SVJ Stochastic volatility jump model

1 Introduction

The objective of this paper is to study the replication and propose a solution to deal with the mark-to-market of complex derivatives contracts exposed to the risk-neutral moments of the SP 500 index, such as the variance contract presented in Bondarenko (2014) [6] and the rare disaster index ($\mathbb{RIX}$) of Gao et al. (2018) [24]. The relevance of such agreements can be driven from a historical perspective by the successions of financial crises: the Asian crisis (1997), Russian crisis (1998), the dot-com bubble (2000), the global financial crisis (2008), and recently, the COVID-19 pandemic (2020). These contracts lack liquidity because they are traded over-the-counter (OTC). This characteristic can create a practical challenge for financial agents exposed to these contracts in their books. The current paper addresses this issue by focusing on replication strategies involving liquid traded assets and by evaluating those contracts with the assistance of the IV parametric model of François et al. (2022) [22].

1.1 Literature Review

For the replication of derivatives contracts, several approaches have been studied in the literature. The first approach is the option tracking, present in Black, Scholes, and Merton (1973) [5], Boyle and Emanuel (1980) [7], Derman and Taleb (2005) [19] and Hull and White (2017) [28]. This approach involves a dynamic rebalancing position in the underlying asset combined with one or two options based on the Greeks. This strategy employs option sensitivities to track the movement of the underlying asset. Therefore, the replication is dependent on the pricing formula which is model-dependent.

The second approach consists of static hedging, as presented in Carr and Madan (1998) [11] and Carr and Wu (2002) [13]. The replication strategy requires a continuum of options with the same time-to-maturity as the derivatives to be hedged. More precisely, static replication involves a buy-and-hold strategy with the purchase of many options at the initial date of the contract. The performance of the replication is directly related to the availability of the options market in terms of strike prices. In contrast to the previous approach, this one is model-free.

The third replication approach found in the literature is the global hedging risk minimization (GHRM). This methodology consists of resolving a replication problem by optimization. The method consists of identifying the self-financing trading strategies that minimize the distance between the payoff and the strategy terminal value. The objective function (the distance) depends on some risk measure. In the work of Xu (2006) [37], the general approach is presented. Civatic and Karatzas (1999) [16] use the expected hedging shortfall, Sekine(2004) [35] minimizes the tail value-at-risk, Remillard and Rubenthaler (2009) [34] consider the expected squared hedging error, and François, Gauthier and Godin (2012) [23] propose an adaptation for regime-switching models.

This research paper aligns itself with the replication method presented in Bondarenko (2014) [6], which falls under the second approach with two replication parts: a static one and a dynamic one. In addition, this thesis answers also the mark-to-market problem for some families of contracts using the continuum of options in the static replication approach. We investigate the limited valuation and replication of such contracts in terms of the availability of a continuous volatility surface. The problem is answered with the use of the implied volatility surface model of François et al. (2022) [22]. In contrast with the

works of Bondarenko (2014) [6] and Gao et al. (2018) [24] that use standard trapezoidal numerical integration. Our approach involves the volatility surface model and answers the discretization error by possibly interpolating/extrapolating the options prices. The convenience of the fitting model is the reliability of its calibration on the risk-neutral volatility surface.

This paper's takeaway can be summarized in two main points. Firstly, it focuses on studying the replication strategy for this product type using liquid traded assets. Secondly, it introduces mark-to-market valuation tools pertinent to the financial agents involved in such derivative contracts. The aim is to provide investors with the opportunity to benefit from convex payoffs (insurance) during extreme events while simplifying the pricing process for these contracts.

This thesis is structured as follows: In Section 2, we provide a historical overview of various strategies employed in trading variances and introduce the contracts under study. Section 3 focuses on the implementation of variance contract replication. Subsection 3.1 presents the data, while subsection 3.2 delves into replicating the variance contract within a Monte Carlo simulation environment. Moving on to Section 3.3, a similar study is conducted using real data. In subsection 3.3.4, we perform a linear regression analysis on the relative errors of our replications. In Section 4, we compare two valuation methods for the contracts: the classical trapezoidal technique and the IV surface model. Subsequently, we present the results of the valuation. Finally, in Section 5, we conclude the thesis.

In summarizing our findings, we note that the methodologies we employ for replicating and valuing our contracts typically produce highly favorable results. However, a limitation arises from a truncation error in the static option portfolio, which is defined by the minimum and maximum strikes available at the inception date. Concerning a small number of replications, this results in a diminished payoff for the static option portfolio, thereby causing a notable difference between the replication and target values.

2 Trading the Variance

In the current section, we present a historical perspective for different variance trading strategies. Our focus is on various measures of the S&P 500 index's variance. Afterward, we introduce classical volatility trading strategies such as the straddle and the variance swap. Finally, we present the risk-neutral contracts based on the work of Bondarenko (2014) [6] and Gao et al. (2018) [24], jointly with the theoretical framework in use for their replication.

2.1 S&P 500 process

The S&P 500 index is the financial market's main benchmark proxy of the US economy, the index is composed of the five hundred most capitalized firms in the New York exchange (NYSE). Another market's proxy is the measure of the volatility of the S&P 500 index quantified by the $\mathbb{VIX}$ index. This index is often seen as the systemic risk indicator or the fear sentiment of the economy. The construction of the $\mathbb{VIX}$ index is closely tied to our variance contract. This relation is detailed in Subsection 2.4.1.

Regarding liquidity, the S&P 500's derivatives follow a specific structure, where futures and options are traded daily. Dewynne and Putyatin (1999) [20] highlight the crucial role of market liquidity in the replication and valuation of derivatives. Consequently, the liquidity of S&P 500's derivatives creates favorable conditions for constructing more complex financial products.

Figures 1 and 2 present the level and the log returns of the S&P 500 index. We observe the time-varying volatility and jumps, especially during financial turmoils.

Consequently, the S&P 500 index dynamics we consider are characterized by stochastic volatility and jumps in index prices.

Let $F_{t,T}$ be the future price at time t of a contract maturity T. As shown in Bates (1996) [3], $\{F_{t,T}\}_{0\leq t\leq T}$ is a $\mathbb{Q}$ martingale. We consider the jump-diffusion dynamics :

$$dF_{t,T} = \sqrt{V_{t^-}} F_{t^-,T} dW_t^{\mathbb{Q}} + F_{t^-,T}\xi_{t^-} dJ_t, \tag{1}$$

where V_t is the stochastic instantaneous variance, $W^{\mathbb{Q}}$ is a Brownian motion under the risk-neutral measure $\mathbb{Q}$ and $\xi_{t^-} dJ_t$ is the finite activity jump component. V_{t^-} is the instantaneous variance, and $F_{t^-,T}$ the future price before the jumps occurrence. Note that $\{J_t\}$ is also a $\mathbb{Q}$ martingale.

Figure 1: Daily S&P 500 level

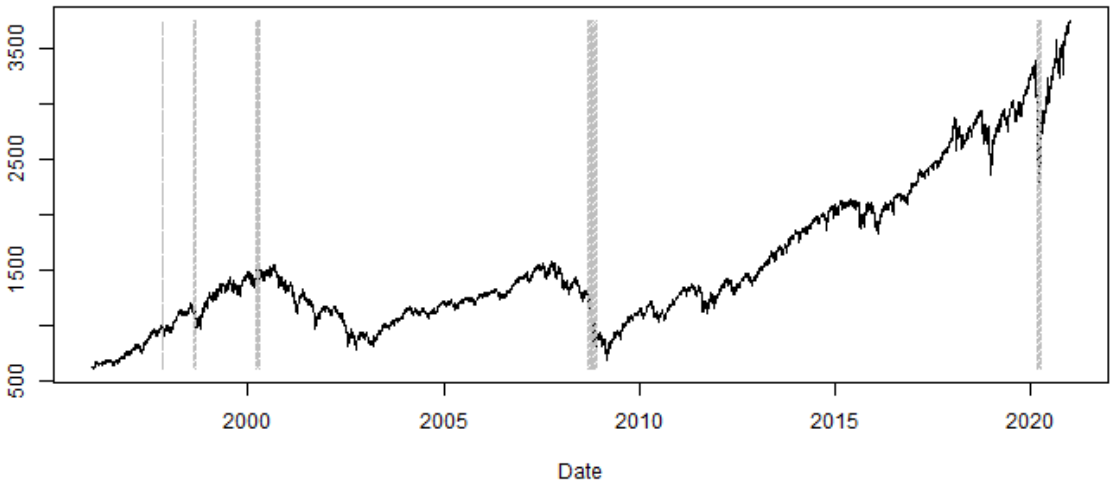

Time series that highlights the impact of the financial crisis on the S&P 500 index from January 1, 1996, to December 31, 2020. The grey shadow highlights key events including the Asian crisis (1997), Russian crisis (1998), dot-com bubble (2000), global financial crisis (2008), and COVID-19 pandemic (2020).

Figure 2: Daily S&P 500 log returns

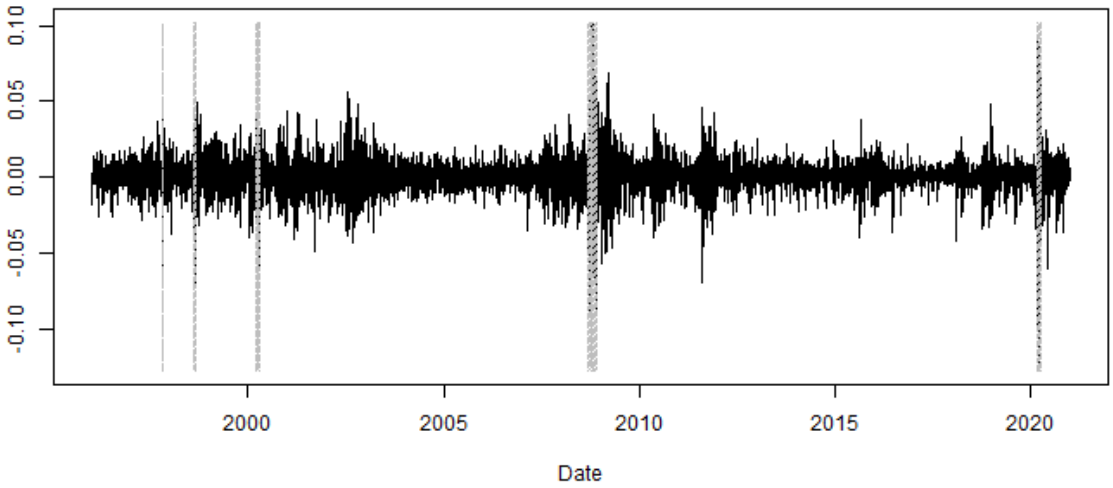

Time series that highlights the impact of financial turmoils on the S&P 500 returns from January 1, 1996, to December 31, 2020. With grey shadow emphasizes the Asian (1997) and Russian crises (1998), the dot-com bubble (2000), the global financial crisis (2008), and the COVID-19 pandemic (2020).

2.2 Classical variance trading strategies

In this subsection, we present well-known trading strategies: the straddle and the variance swap. This brief presentation of those classical volatility trading strategies provides an intuitive historical perspective for the construction of the derivative present in Section 2.4.

2.2.1 Straddle

We begin with the simplest trading strategy involving the variance (volatility) exposure: the straddle. It consists of buying a European call and a European put with the same maturity and strike price. The straddle payoff is

$$\Pi_t^{straddle} = (S_t - K)^+ + (K - S_t)^+.$$

The combination of put and call can be viewed as a positive exposition on the large movement of an asset. We can imagine a trader involved in an at-the-money straddle (i.e., the strike equals the spot price). With this consideration, if the index moves largely away from its initial price, the payoff of the straddle gives a positive gain (i.e., is in-the-money). In contrast, if the underling asset does not move significantly during the contract maturity, the straddle gives a small payoff, and the net profit is negative. An investor expecting a large move can then be long on a straddle, precisely by the non-directional profile of this trading position. A brief description of the payoff and dynamics is presented in Figure 3 and is taken from Hull (2018) [27].

Figure 3: Payoff of straddle

Figure 12.10 Profit from a straddle.

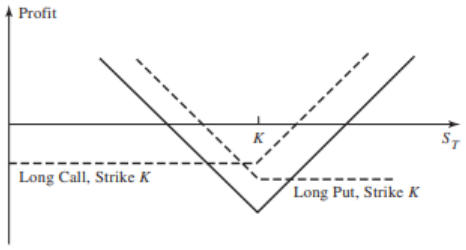

Table 12.5 Payoff from a straddle.

Range of stock price	*Payoff from call*	*Payoff from put*	*Total payoff*
$S_T \leqslant K$	0	$K - S_T$	$K - S_T$
$S_T > K$	$S_T - K$	0	$S_T - K$

Hull, Options, Futures and Other Derivatives. 9th Global Edition, p.267 [27]

Figure 3 represents the profit of the straddle strategy. The financial agents involved in this strategy are subject to only the cost of the call and the put at initiation. The straddle profit becomes

$$Profit_t^{straddle} = (S_t - K)^+ + (K - S_t)^+ - C(S_t, K, T) - P(S_t, K, T).$$

Some more flexible extensions of the straddle exist commonly called a strip, a strap, and a strangle. Those types of contracts are replicated by a dynamic hedging strategy.

2.2.2 Variance swap

Another related contract is the variance swap introduced by Carr and Madan (1998) [11]. A variance swap is a contract that allows an investor to hedge or speculate on the variance of an underlying asset. Precisely, this agreement allows us to gain exposure to the future realized variance. The payoff of the contract relies on the difference between the realized variance and a fixed variance strike set at the contract inception date $h_0 = 0$. The realized variance is computed based on the historical returns of the underlying asset.

The realized variance RV_H is calculated on the swap's reference period $[0, H]$.

For $0 = h_0 < h_i < ... < h_n = H$,

$$RV_H = \sum_{i=1}^{H} \left(\ln \left(\frac{F_{h_i,H}}{F_{h_{i-1},H}} \right) \right)^2,$$

where RV_H is the approximation of the quadratic variation and H is the swap maturity date on 365-day basis.

Typically, annualized RV_H represents the floating leg of the variance swap. The fixed leg represents the fixed variance strike at the inception of the swap.

Considering these swap's legs settings, the variance swap settlement payoff Π_H^{VS} is

$$\Pi_H^{VS} = N_{VS} \left(RV_H - K_{0,H}^{VS} \right),$$

where N_{VS} is the cash notional of the swap settlement and $K_{0,H}^{VS}$ is the fixed variance strike.

The fair strike $K_{0,H}^{VS}$ is obtained by setting the risk-neutral expectation of the payoff at the swap's inception to zero,

$$\mathbb{E}_0^{\mathbb{Q}} \left[N_{VS} \left(RV_H - K_{0,H}^{VS} \right) \right] = 0,$$

which implies that

$$K_{0,H}^{VS} = \mathbb{E}_0^{\mathbb{Q}} \left[RV_H \right] \cong \mathbb{E}_0^{\mathbb{Q}} \left[QV_H \right],$$

where QV_H is the quadratic variation on the futures contract over $[0, H]$. Therefore, the fixed strike price is defined as the risk-neutral expectation of the quadratic variation.

At the swap's maturity H, if $RV_H > K_{0,H}^{VS}$ the holder of the swap receive the cash settlement. In case $RV_H < K_{0,H}^{VS}$, the holder of the swap will pay the cash settlement. It's important to note that the variance swap differs from the straddle. Unlike the straddle, which is limited to the options costs, the variance swap may result in a negative cash flow, and the swap holder may face margin calls if a significant loss occurs during the swap's life.

2.3 Carr-Madan Framework

In the current subsection, we present the Carr-Madan framework. This framework is the main tool for the static replication of Bondarenko's quadratic variation payoff Bqv_T.

Carr and Madan (1998) [11], propose a static replication strategy based on many positions in the option market. The strategy involves adopting a buy-and-hold approach, where the initial investment occurs at the starting date $t_0 = 0$, and all payoffs are received at the terminal date t. The framework relies on the existence of a continuum of strike prices for European options.

In Carr Madan (1998) [11], for any twice differentiable function g, the payoff $g(F_{t,T})$ is replicated by a static portfolio made from a position in a bank account, a futures contract and a portfolio of put and call options :

$$g(F_{t,T}) = g(F_{0,T}) + g'(F_{0,T})(F_{t,T} - F_{0,T}) + \int_0^{F_{0,T}} g''(K)(K - F_{t,T})^+ dK + \int_{F_{0,T}}^{\infty} g''(K)(F_{t,T} - K)^+ dK, \tag{2}$$

where $g'(K)$ and $g''(K)$ are the first and second derivatives of $g(K)$. The first term mimics the static position of a pure discount bond that pays $g(F_{0,T})$ at t. The second term is the payoff from $g'(F_{0,T})$ of the amplitude between the terminal and initiation values of the futures price. The third and fourth terms are the terminal payoff of the European calls and puts.

This strategy for replication, being model-free, operates without being confined by assumptions about the market structure. The fact that no underlying asset price dynamics hypothesis is needed provides some robustness to the trading strategy.

However, there is a limitation to this approach. In practice, the absence of a continuum of strike prices and maturities restricts a straightforward application of the static replicating portfolio. The presence of these constraints poses a challenge in replicating the variance contract, particularly involving an error in terms of the truncation and the discretization scale of the integrals.

2.4 Risk-neutral contracts

In the current subsection, we present the different risk-neutral contracts obtained as the special cases of the Carr-Madan formula shown in Equation (2).

2.4.1 Variance contract

The contract's payoff is contingent on the quadratic variation of the futures price over the period $[t, T]$. Using the Carr-Madan formula, the replication of this payoff involves employing a variety of European puts and calls. The details of this replication process are explained below.

The variance contract relies on the following derivations involving Equation (1) which presents the future's stochastic differential equation.

Itô's lemma leads to

$$\begin{aligned}\ln(F_{t,T}) &= \ln(F_{0^+,T}) + \int_{0^+}^{t} \frac{1}{F_{u^-,T}} dF_{u,T} - \frac{1}{2}\int_{0^+}^{t} \frac{1}{F_{u,T}^2} d\langle F_{u,T}\rangle \\ &\quad + \sum_{0^+<u\leq t} \{\ln(F_{u,T}) - \ln(F_{u^-,T}) - \frac{1}{F_{u^-,T}}\Delta F_{u,T}\}. \\ &= \ln(F_{0^+,T}) + \int_{0^+}^{t} \frac{1}{F_{u^-,T}} dF_{u,T} - \frac{1}{2}\int_{0^+}^{t} V_{u^-} du + \sum_{0^+<u\leq t} \{\ln(1+\xi_u \Delta J_u) - \xi_{u^-}\Delta J_u\},\end{aligned}$$

where $\Delta F_{u,T} = F_{u,T} - F_{u^-,T}$.

A Taylor expansion of $\ln(1+\xi_u \Delta J_u)$ around $\xi_u \Delta J_u$ for the jump component gives

$$\sum_{0^+<u\leq t} \{\ln(1+\xi_u \Delta J_u) - \xi_{u^-}\Delta J_u\} \cong \sum_{0^+<u\leq t} \left\{\xi_{u^-}\Delta J_u + \frac{1}{2}\xi_{u^-}^2 (\Delta J_u)^2 - \xi_{u^-}\Delta J_u\right\}.$$

Therefore,

$$\ln(F_{t,T}) \cong \ln(F_{0^+,T}) + \int_{0^+}^{t} \frac{1}{F_{u^-,T}} dF_{u,T} - \frac{1}{2}\int_{0^+}^{t} V_{u^-} du - \sum_{0^+<u\leq t} \frac{1}{2}\xi_{u^-}^2 (\Delta J_u)^2.$$

Let $0 = t_0 < t_i < ... < t_n = T$, with $\lim_{n\to\infty} \max_{i\in\{1,...,n\}} (t_i - t_{i-1}) = 0$.

$$\begin{aligned}\int_{0^+}^{t} V_{u^-} du + \sum_{0^+<u<t} \frac{1}{2}\xi_{u^-}^2 (\Delta J_u)^2 &\cong 2\left\{\int_{0^+}^{t} \frac{1}{F_{u^-,T}} dF_{u,T} - \ln\left(\frac{F_{t,T}}{F_{0^+,T}}\right)\right\}, \\ &\cong 2\left\{\sum_{i=1}^{n} \frac{F_{t_i,T} - F_{t_{i-1},T}}{F_{t_{i-1},T}} - \sum_{i=1}^{n} \ln\left(\frac{F_{t_i,T}}{F_{t_{i-1},T}}\right)\right\}. \qquad (3)\end{aligned}$$

The left-hand side Equation of (3) corresponds to the quadratic variation of the log future. Therefore, the right-hand side of the Equation (3) can be interpreted as an observable proxy of the quadratic variation.

By Equation (3), we define the "Bondarenko's quadratic" variation Bqv_T. This measure is path-dependent from $t_0 = 0$ to the future's expiry T.

$$Bqv_T = 2\left\{\sum_{i=1}^{n} \frac{F_{t_i,T} - F_{t_{i-1},T}}{F_{t_{i-1},T}} - \sum_{i=1}^{n} \ln\left(\frac{F_{t_i,T}}{F_{t_{i-1},T}}\right)\right\}. \qquad (4)$$

Using the Carr-Madan formula (1998),

$$g(F_{t,T}) = g(F_{0,T}) + g'(F_{0,T})(F_{t,T} - F_{0,T}) + \int_0^{F_{0,T}} g''(K)(K - F_{t,T})^+ dK + \int_{F_{0,T}}^{\infty} g''(K)(F_{t,T} - K)^+ dK.$$

When $g(F_{t,T}) = \ln(F_{t,T})$, the expression becomes

$$\ln(F_{t,T}) = \ln(F_{0,T}) + \frac{1}{F_{0,T}}(F_{t,T} - F_{0,T}) - \int_0^{F_{0,T}} \frac{1}{K^2}(K - F_{t,T})^+ dK - \int_{F_{0,T}}^{\infty} \frac{1}{K^2}(F_{t,T} - K)^+ dK. \tag{5}$$

which leads to

$$\begin{aligned} & 2\left\{\int_0^{F_{0,T}} \frac{1}{K^2}(K - F_{t,T})^+ dK + \int_{F_{0,T}}^{\infty} \frac{1}{K^2}(F_{t,T} - K)^+ dK\right\} \\ & = 2\left(\frac{F_{t,T} - F_{0,T}}{F_{0,T}}\right) - 2\ln\left(\frac{F_{t,T}}{F_{0,T}}\right). \\ & = 2\sum_{i=1}^{n} \frac{F_{t_i,T} - F_{t_{i-1},T}}{F_{t_{i-1},T}} - 2\sum_{i=1}^{n} \ln\left(\frac{F_{t_i,T}}{F_{t_{i-1},T}}\right) \\ & + 2\sum_{i=1}^{n}\left\{\frac{F_{t_i,T} - F_{t_{i-1},T}}{F_{0,T}} - \frac{F_{t_i,T} - F_{t_{i-1},T}}{F_{t_{i-1},T}}\right\}. \end{aligned} \tag{6}$$

Therefore,

$$\begin{aligned} Bqv_T &= \sum_{i=1}^{n} \frac{F_{t_i,T} - F_{t_{i-1},T}}{F_{t_{i-1},T}} - 2\sum_{i=1}^{n} \ln\left(\frac{F_{t_i,T}}{F_{t_{i-1},T}}\right) \\ &= 2\left\{\int_0^{F_{0,T}} \frac{1}{K^2}(K - F_{t,T})^+ dK + \int_{F_{0,T}}^{\infty} \frac{1}{K^2}(F_{t,T} - K)^+ dK\right\} \\ &+ 2\sum_{i=1}^{n}\left(\frac{1}{F_{t_{i-1},T}} - \frac{1}{F_{0,T}}\right)(F_{t_i,T} - F_{t_{i-1},T}). \end{aligned}$$

This results in the variance contact Bqv_T payoff in terms of the following replication strategy,

$$\begin{aligned} Bqv_T &\cong \underbrace{2\left\{\int_0^{F_{0,T}} \frac{1}{K^2}(K - F_{t,T})^+ dK + \int_{F_{0,T}}^{\infty} \frac{1}{K^2}(F_{t,T} - K)^+ dK\right\}}_{\text{Option portfolio } OP_T} \\ &+ \underbrace{2\sum_{i=1}^{n}\left(\frac{1}{F_{t_{i-1},T}} - \frac{1}{F_{0,T}}\right)\left(F_{t_i,T} - F_{t_{i-1},T}\right)}_{\text{Dynamical strategy } DS_T}. \\ &= OP_T + DS_T. \\ &= RP_T. \end{aligned} \tag{7}$$

DS_T represents the dynamic trading strategy, and OP_T is the options portfolio. In theory, RP_T acts as the replication portfolio, but practical limitations prevent access to a continuum of strike prices. Furthermore, it's important to observe that the expiration date T for the future $F_{t,T}$ aligns with the expiration date for the terminal payoff of the options.

The initial mark-to-market valuation of the static buy and hold position depends on the options prices $P(F_{t,T}, K, T)$ and $C(F_{t,T}, K, T)$. This valuation consists of the discounted risk-neutral expectation of the Equation (7) at $t_0 = 0$,

$$\mathbb{E}_0^{\mathbb{Q}}\left[e^{-rT} RP_T\right] = 2\left\{\int_0^{F_{0,T}} \frac{1}{K^2} P(F_{0,T}, K, T)dK + \int_{F_{0,T}}^{\infty} \frac{1}{K^2} C(F_{0,T}, K, T)dK\right\}. \tag{8}$$

The risk-neutral expectation of the dynamical strategy DS_T is zero because of the martingale property

$$\begin{aligned}
&\mathbb{E}_0^{\mathbb{Q}}\left[\sum_{i=1}^{n}\left(\frac{1}{F_{t_{i-1},T}} - \frac{1}{F_{0,T}}\right)\left(F_{t_i,T} - F_{t_{i-1},T}\right)\right]. \\
&= \sum_{i=1}^{n} \mathbb{E}_0^{\mathbb{Q}}\left[\mathbb{E}_0^{\mathbb{Q}}\left[\left(\frac{1}{F_{t_{i-1},T}} - \frac{1}{F_{0,T}}\right)\left(F_{t_i,T} - F_{t_{i-1},T}\right)\right]\middle| F_{t_{i-1}}\right]. \\
&= \sum_{i=1}^{n} \mathbb{E}_0^{\mathbb{Q}}\left[\left(\frac{1}{F_{t_{i-1},T}} - \frac{1}{F_{0,T}}\right)\underbrace{\mathbb{E}_0^{\mathbb{Q}}\left[\left(F_{t_i,T} - F_{t_{i-1},T}\right)\middle| F_{t_{i-1}}\right]}_{=0 \text{ because } F_{t_i,T} \text{ is a martingale}}\right].
\end{aligned}$$

Concerning the costs associated with this contract, the financial agent must pay the price of OP_T at $t_0 = 0$. Furthermore, replicating the contract incurs additional costs related to the daily rebalancing of the dynamic trading strategy, which varies by the daily futures price.

As mentioned earlier in Section 2.1, there is an analogy to make with the well-known $\mathbb{VIX}$ index. In fact, the $\mathbb{VIX}$ relies on the variance contract. With T equal 30/365 (30 days) and r the risk-free rate.

The index is derived using $\mathbb{E}_0^{\mathbb{Q}}\left[e^{-rT} RP_T\right]$ along with a multiplicative factor,

$$\mathbb{VIX} = 100 \times \sqrt{\frac{2e^{rT}}{T}\left\{\int_0^{F_{0,T}} \frac{1}{K^2} P(F_{0,T}, K, T)dK + \int_{F_{0,T}}^{\infty} \frac{1}{K^2} C(F_{0,T}, K, T)dK\right\}}. \tag{9}$$

2.4.2 Rare disaster index ($\mathbb{RIX}$)

In the study by Gao et al. (2018) [24], an additional significant financial instrument is introduced, referred to as the "rare disaster index." This index adopts a methodology similar to Bondarenko's (2014) [6] variance contract but distinguishes itself through its capability to capture extreme downside market shocks. The $\mathbb{RIX}$ is formulated based on the spread between two options portfolios, as detailed in Appendix A. The first portfolio, denoted as Π_t^{1-}, represents the left-tail risk-neutral variance, also identified as $\widehat{JTIX^-}$ in

Du and Kapadia's analysis (2012) [21].

$$\mathbb{E}_0^{\mathbb{Q}}\left[e^{-rT}\left(\ln\frac{F_{t,T}}{F_{0,T}}\right)^2\right]^- = \Pi_t^{1-} = 2\left\{\int_0^{F_{0,T}} \frac{\left(1-\ln\left(\frac{K}{F_{0,T}}\right)\right)}{K^2} P(F_{0,T},K,T)\,dK\right\}. \quad (10)$$

The second portfolio, Π_t^{2-}, closely resembles our variance contract portfolio, with the key distinction being the inclusion of only the left tail. As outlined by Gao et al. (2018) [24], this portfolio is designed to capture a moderate volatility shock in the market.

$$\mathbb{E}_0^{\mathbb{Q}}\left[e^{-rT}Bqv_T\right]^- = \Pi_t^{2-} = 2\left\{\int_0^{F_{0,T}} \frac{1}{K^2} P(F_{0,T},K,T)\,dK\right\}. \quad (11)$$

The formulation of the options portfolio as described in Equation (10) differs from that in Equation (11) by assigning higher weights to significantly out-of-the-money puts. As the strike decreases, the put option moves further out-of-the-money. The negative indicator $^-$ specifies that only puts are taken into account. Furthermore, this portfolio exhibits a directional nature compared to the one presented in Section 2.4.1.

The $\mathbb{RIX}$ is defined by the spread between the Equations (10) and (11)

$$\mathbb{RIX} = \Pi_t^{1-} - \Pi_t^{2-} = 2\left\{\int_0^{F_{0,T}} \frac{\ln\left(\frac{F_{0,T}}{K}\right)}{K^2} P(F_{0,T},K,T)\,dK\right\}. \quad (12)$$

The derivations are found in Appendix A.

3 Implementation

3.1 Data

The financial data indicators are the European options of the S&P 500 index, the future prices, and the treasury risk-free rate (1 month to 3 years). The OptionMetrics database is the source for the futures and options prices. For the risk-free rate, we obtain the treasury rates, available on the FRED database. The methodology used for the data matching of those three variables is the same as in François et al. (2022) [22]. The matching consists of having the same expiration date for the futures and the options. For the risk-free rate, we use the closest one associated with the respected maturity of the derivatives. The data timeline is from January 4, 1996, to December 31, 2020.

Table 1: Descriptive statistics of the S&P 500 volatility surface by moneyness (i.e, puts with $M > 0$ and calls with $M < 0$)

	Calls and Puts					
	$M \leq -0.2$	$-0.2 < M \leq 0$	$0 < M \leq 0.2$	$0 < M \leq 0.2$	$M > 0.8$	All
Average IV (%)	19.61	14.45	19.28	28.28	48.18	24.52
Standard deviation IV (%)	9.63	6.41	6.94	7.75	13.59	12.45
Number of contracts	671,917	1,859,798	1,945,186	3,441,450	815,069	8,733,420

Descriptive statistics of the daily S&P 500 options implied volatility (IV) surfaces from January 4, 1996, to December 31, 2020, grouped by buckets of moneyness. M is the moneyness computed in Equation (38)

As shown in Table 1, our sample is composed of around 30% OTM calls and 70% OTM puts. The average implied volatility for the puts is also higher than the one of the calls. This asymmetry in terms of the implied volatility has a direct consequence on the payoff of the static option portfolio OP_T. Moreover, in scenarios where there are fewer calls than puts, there exists the potential of not capturing positive jumps in the options portfolio OP_T for a given inception date.

We illustrate this disparity in the time series for the number of contracts, as shown in Figures 4 and 5. Throughout our sample period from January 1996 to December 2020, we observe an increase in the quantity of out-of-the-money (OTM) options in recent years. However, it is evident that the numbers of calls consistently remain lower than the numbers of puts.

Finally, Figures 6 and 7 present the time series of the average strike distance at t_0 for each maturity.

Figure 4: Time series of the quantity of the market's call options

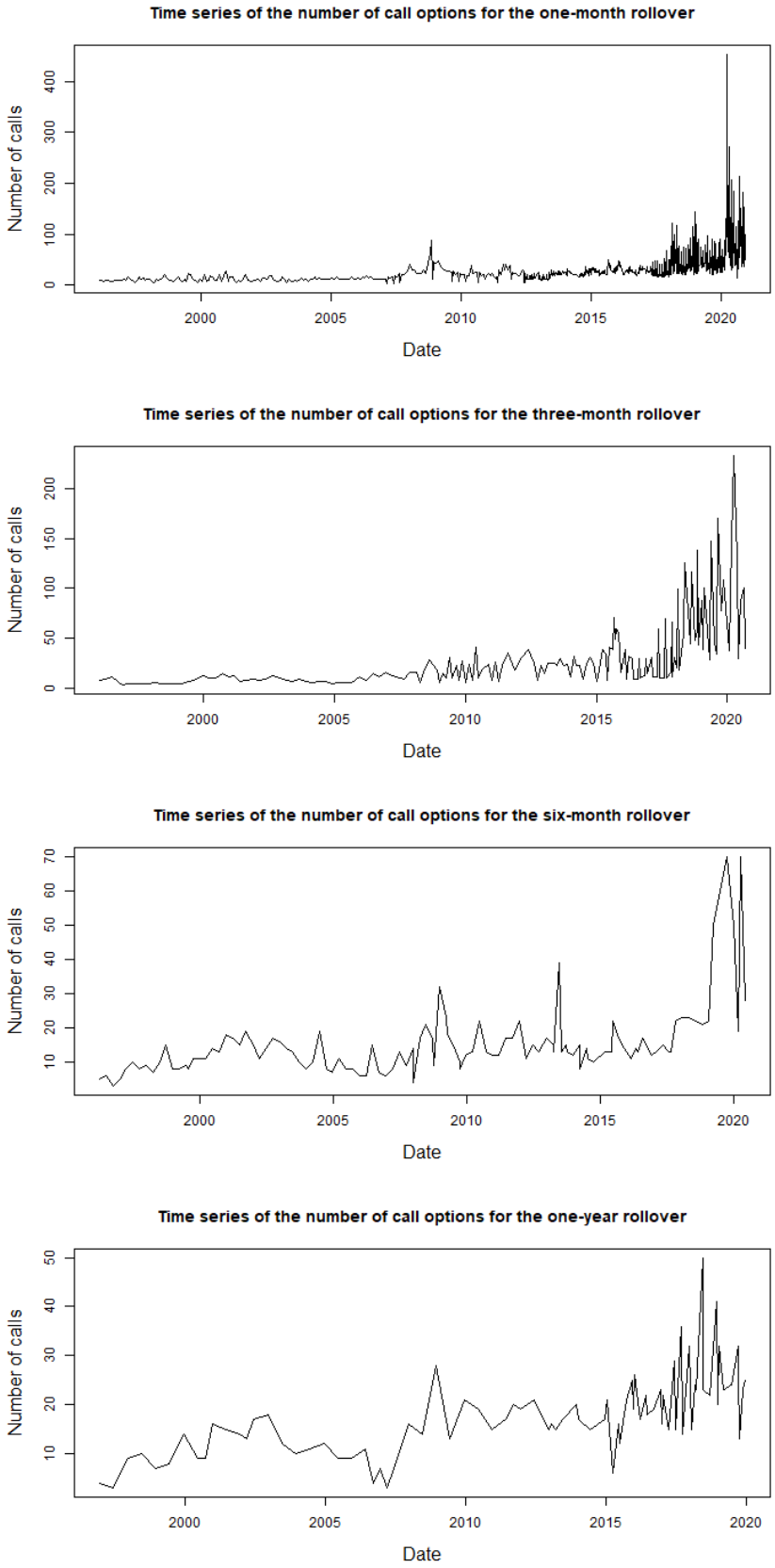

Time series of the number of calls for the different roll-overs across our sample, beginning from January 1996 to December 2020.

Figure 5: Time series of the quantity of the market's put options

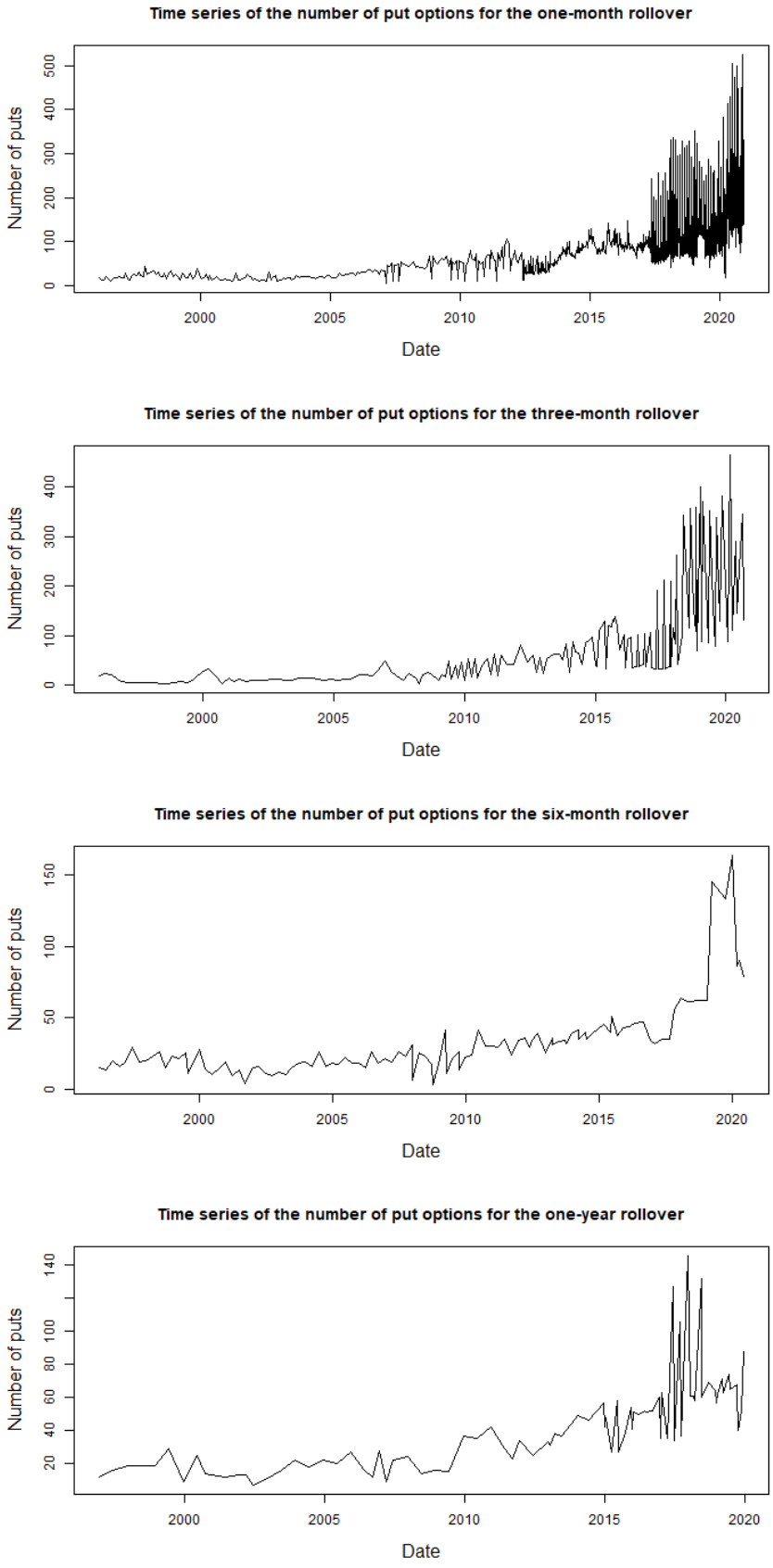

Time series of the number of puts for the different roll-overs across our sample, beginning from January 1996 to December 2020.

Figure 6: Time series of the average strike distance ΔK of the market's put options

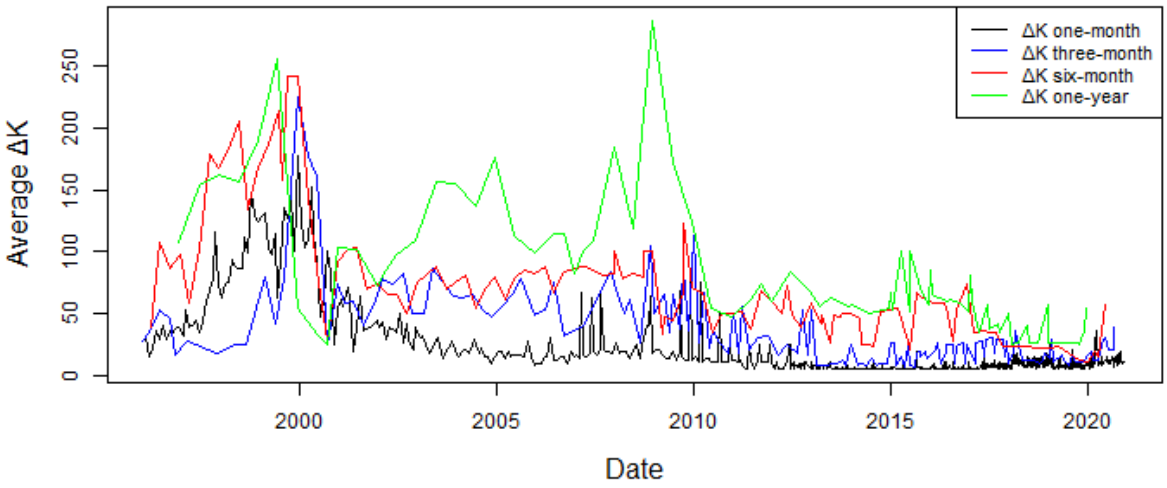

Time series of the average ΔK for the puts, obtained by calculating the daily arithmetic average of the strike distance across all maturities.

Figure 7: Time series of the average strike distance ΔK of the market's call options

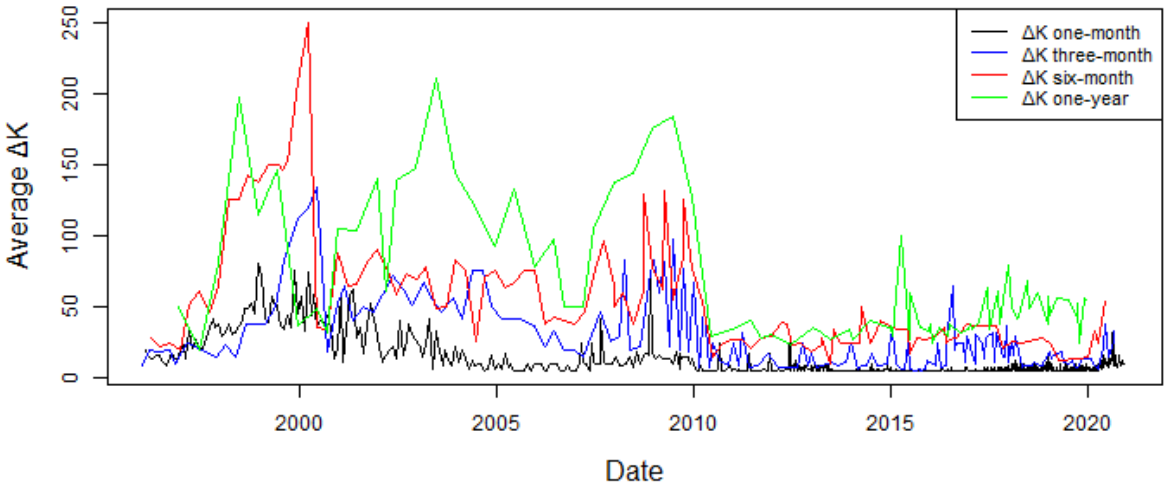

Time series of the average ΔK for the calls, obtained by calculating the daily arithmetic average of the strike distance across all maturities.

3.2 Monte Carlo study

In this section, we present simulations to replicate the payoff Bqv_T of the variance contract. First, in Subsection 3.2.1, we outline the model characteristics and how it is discretized. Next, we explain the use of the trapezoidal method to evaluate the static portfolio OP_T payoff, discussing sources of errors such as discretization scale and truncation error. Thirdly, we provide a concise overview of the simulation's implementation. Finally, we present simulation results, including a series of tests to determine whether the replication error is primarily due to the discretization scale or the truncation error.

3.2.1 The Stochastic volatility Jump Model

In this current subsection, we are considering the log price of the S&P 500 index and the following jump-diffusion process as the one presented in the Bates model [3], under the physical measure.

$$
\begin{aligned}
dY_t &= \left(r + \eta V_t - \lambda \mathbb{E}(e^{\xi_{t^-}} - 1)\right) dt + \sqrt{V_t} dW^{\mathbb{P}}_{Y_t} + \xi_{t^-} dJ_t. \\
dV_t &= \kappa \left(\theta - V_t\right) dt + \sigma \sqrt{V_t} dW^{\mathbb{P}}_{V_t}.
\end{aligned}
$$

The future contract in terms of the log prices is obtained through the cash-and-carry relation $F_{t,T} = \exp\{Y_t + r(T-t)\}$ where r is the risk-free rate, η is the equity risk premium parameter, κ is the mean-reversion speed of the variance process, θ is the long-run variance level, V_t is the instantaneous variance and σ is the volatility of the volatility. J_t represents a Poisson process with intensity λ, and the jump size ξ_{t^-} are normally distributed with expectation μ_{ξ_t} and standard deviation σ_{ξ_t} i.e., $\xi_{t^-} \sim N(\mu_{\xi_t, \sigma_{\xi_t}})$. $\{J_t\}_{t \geq 0}$ is independent of the two Brownian motions and the jump sizes. The Brownian motions are correlated with a correlation coefficient ρ i.e., $\text{Corr}(W^{\mathbb{P}}_{Y_t}, W^{\mathbb{P}}_{V_t}) = \rho$. And $\mathbb{E}(e^{\xi_{t^-}}) = e^{\mu_{\xi_t} + \frac{1}{2}(\sigma_{\xi_t})^2}$.

3.2.1.1 Model discretization

The model is simulated with the Euler approximation scheme. The time step size is $\Delta t \cong T/n$, where T is the future's maturity and n is the number of the simulated steps (per paths)[1]. For the variance process, we apply the rule $V_t^+ = (V_t, 0)^+$ by taking into consideration only the positive terminal variance.

We capture the correlation between the Brownian motions by the Cholesky decomposition: $\rho Z_1 + \sqrt{1-\rho^2} Z_2$, where Z_1 and Z_2 are respectively two independent standard normal random variables and ρ is the correlation coefficient.

For the jump part, J follows a Poisson distribution with a parameter $\lambda \Delta t$, capturing the discrete occurrences of jumps within the time step Δt. The individual jump magnitudes, X_i, are drawn from a normal distribution with a mean of μ_{ξ_t} and a standard deviation of σ_{ξ_t}. Consequently, the cumulative impact of these jumps is discretely approximated as the sum $\sum_{i=1}^{J} X_i$.

In addition $Y_{t+\Delta}$ is the log stock price, $F_{t+\Delta t,T}$ the futures contract price.

[1] The value of n is 30 days.

Following the Euler approximation, the model is

$$\begin{aligned}
\Delta t &\cong T/n. \\
V_{t+\Delta t} &\cong V_t + \kappa\left(\theta - V_t^+\right)\Delta t + \sigma\sqrt{V_t^+\Delta t}\left(\rho Z_1 + \sqrt{1-\rho^2}Z_2\right). \\
Y_{t+\Delta t} &\cong Y_t + \left(r + \eta V_t^+ - \lambda\left(e^{\mu_{\xi_t}+\frac{1}{2}\sigma_{\xi_t}^2}\right)\right)\Delta t + \sqrt{V_t^+\Delta t}Z_1 + \sum_{i=1}^{J} X_i. \\
F_{t+\Delta t,T} &\cong \exp\left(Y_{t+\Delta t}\, e^{r\Delta t}\right).
\end{aligned}$$

3.2.1.2 Simulation Parameters

We use the same parameters estimated in Bégin and Gauthier (2020)[4].

Table 2: Parameters for the SVJ model used for the simulation study.

Parameter	Value
κ	5.130
θ	0.044
σ	0.520
ρ	-0.754
μ_{ξ_t}	-0.025
σ_{ξ_t}	0.040
η	2.526
λ	1.512
n	30
Δt	1/365
r	1.54%

κ is the mean-reversion speed of the variance process, θ is the long run variance level, σ is the volatility of the volatility, ρ is the two Brownian correlation coefficient and η is equity premium risk parameter. For the jump part, the intensity is λ with a normally distributed jump size ξ_{t^-} with expectation μ_{ξ_t} and standard deviation σ_{ξ_t}. Additionally, n is the number of scheme step, Δt is the time step size and r is the risk-free rate.

3.2.2 Strategies replications

To replicate the payoff Bqv_T, a necessary condition is the existence of a portfolio of options OP_T that is constructed on a continuum of the strikes. However, in practice, there is no existence of such a continuum. To evaluate Equation (7), we use a numerical integration method : the trapezoidal rule. In our simulations, we evaluate the numerical value of OP_T based on the payoffs of the calls and puts at maturity T. The portfolio weights rely on the available strikes at $t_0 = 0$. Additionally, the current future price $F_{0,T}$ serves as an input for defining the integral bounds, while the terminal future price $F_{t,T}$ is used for computing options payoffs at maturity T. The emphasis in this section lies in the payoff replication, thereby eliminating the necessity of options prices.

We evaluate the portfolio OP_T by considering the discrete grid with N equally spaced strike prices

$$K_1 < ... < K_{k-1} < F_{0,T} < K_k < ... < K_N,$$

and we define $\Delta K_i = K_{i+1} - K_{i-1}$ for $2 \leq i \leq N-1$, $\Delta K_1 = K_2 - K_1$ and $\Delta K_N = K_N - K_{N-1}$.

The approximation of the payoff for the puts leads to

$$\int_0^{F_{0,T}} \frac{1}{K^2}(K - F_{t,T})^+ dK \cong \sum_{i=1}^{k-1} \frac{1}{2}\frac{\Delta K_i}{K_i^2}\left(K_i - F_{t,T}\right)^+. \tag{13}$$

The approximation of the payoff for the calls leads to

$$\int_{F_{0,T}}^{\infty} \frac{1}{K^2}(F_{t,T} - K)^+ dK \cong \sum_{i=k}^{N} \frac{1}{2}\frac{\Delta K_i}{K_i^2}\left(F_{t,T} - K_i\right)^+. \tag{14}$$

In the case $K_1 < ... < K_{k-1} \leq F_{0,T} < K_k < ... < K_N$ a correction is required around $F_{0,T}$,

The correction of the payoff for the puts leads to

$$\begin{aligned}\int_0^{F_{0,T}} \frac{1}{K^2}(K - F_{t,T})^+ dK &= \int_0^{K_1} \frac{1}{K^2}(K - F_{t,T})^+ dK + \int_{K_1}^{K_{k-1}} \frac{1}{K^2}(K - F_{t,T})^+ dK \\ &\quad + \int_{K_{k-1}}^{F_{0,T}} \frac{1}{K^2}(K - F_{t,T})^+ dK. \\ &\cong \sum_{i=2}^{k-1} \int_{K_{i-1}}^{K_i} \frac{1}{K^2}(K - F_{t,T})^+ dK.\end{aligned}$$

The correction of the payoff for the calls leads to

$$\begin{aligned}\int_{F_{0,T}}^{\infty} \frac{1}{K^2}(F_{t,T} - K)^+ dK &= \int_{F_{0,T}}^{K_k} \frac{1}{K^2}(F_{t,T} - K)^+ dK + \int_{K_k}^{K_N} \frac{1}{K^2}(F_{t,T} - K)^+ dK \\ &\quad + \int_{K_N}^{\infty} \frac{1}{K^2}(F_{t,T} - K)^+ dK. \\ &\cong \sum_{i=k+1}^{N} \int_{K_{i-1}}^{K_i} \frac{1}{K^2}(F_{t,T} - K)^+ dK.\end{aligned}$$

It's important to note that the increment $\Delta K_i = \frac{K_N - K_1}{N}$ in each integral. We choose these bounds by setting K_1 as the lower bound and K_N as the upper one, which are respectively the minimum and maximum of the available strike grid at each replication's inception date t_0. For simulation purposes, it is assumed that ΔK_i remains constant. As the value of N increases, the accuracy of approximations improves, leading to a reduction in the value of ΔK_i. In simpler terms, a higher N leads to a more refined discretization, thereby enhancing the precision of the calculations.

The precision is also influenced by truncation errors associated with the lower bound in Equation (13) for put payoffs and the upper bound in Equation (14) for call payoffs. Consequently, the option's payoff is directly impacted by the distance between K_1 and K_N from $F_{0,T}$, particularly during periods of higher volatility in the underlying asset.

Therefore combining Equations (13) and (14)

$$OP_T = 2\left\{\sum_{i=1}^{k-1}\frac{1}{2}\frac{\Delta K_i}{K_i^2}\left(K_i - F_{t,T}\right)^+ + \sum_{i=k}^{N}\frac{1}{2}\frac{\Delta K_i}{K_i^2}\left(F_{t,T} - K_i\right)^+\right\}. \tag{15}$$

Concerning the dynamic strategy DS_T, we adjust our position on a daily frequency based on the trajectory of $F_{t,T}$. The position is determined by calculating $\left(\frac{1}{F_{t_{i-1},T}} - \frac{1}{F_{0,T}}\right)$ for each day t.

3.2.3 Simulations

In this subsection, our primary objective is to assess the resilience of our replication portfolio RP_T within a singular 30-day strategy horizon. To achieve this, we conduct simulations on 100,000 paths of the process to determine the terminal price $F_{t,T}$. Upon maturity, for each path j, we compute the spread between our replication portfolio RP_T and the target payoff Bqv_T. For a more in-depth understanding of the implementation, the pseudo-algorithm is available in Appendix B.

We begin by simulating our paths with the following characteristics. The initial future price $F_{0,T} = 3257.75$, the risk-free rate $r = 1.54\%$, which are observable in the beginning of January 2020 (2020-01-02), the instantaneous variance $V_0 = 4.4\%$, and the maturity $T = 30/365$. The time step Δt of the simulation is $1/365$, with n being one day. For each path j, we compute Equation (4), the target payoff Bqv_T. We also calculate the two parts of Equation (7). The static OP_T payoff is obtained by Equation (15). The dynamical strategy DS_T is rebalancing daily $\left(\frac{1}{F_{t_{i-1},T}} - \frac{1}{F_{0,T}}\right)$ shares at every step n. With the addition of those two terms, we obtain the replication payoff RP_T. We observe that the values of Bqv_T and RP_T are small. To address this issue, we have opted to apply a scaling transformation to both variables, denoted as $sBqv_T$ and sRP_T. This type of transformation is akin to the one employed for the $\mathbb{VIX}$ index, as we show in Equation (9). Through this application, we apply normalization in terms of percentage and maturity simply for aesthetic scaling purposes. Finally, by construction $\text{RRMSE} = \sqrt{\frac{1}{n}\sum_{j=1}^{n}\left(\epsilon^{(j)}\right)^2}$, representing the Relative Root-Square Mean Error of the replication.

$$Bqv_T^{(j)} = 2\left\{\sum_{i=1}^{n}\frac{F_{t_i,T}^{(j)} - F_{t_{i-1},T}^{(j)}}{F_{t_{i-1},T}^{(j)}} - \sum_{i=1}^{n}\ln\left(\frac{F_{t_i,T}^{(j)}}{F_{t_{i-1},T}^{(j)}}\right)\right\}. \tag{16}$$

$$OP_T^{(j)} = 2\left\{\sum_{i=1}^{k-1}\frac{\Delta K_i}{K_i^2}\left(K_i - F_{t,T}^{(j)}\right)^+ + \sum_{i=k}^{N}\frac{\Delta K_i}{K_i^2}\left(F_{t,T}^{(j)} - K_i\right)^+\right\}. \tag{17}$$

$$DS_T^{(j)} = 2\sum_{i=1}^{n}\left(\frac{1}{F_{t_{i-1},T}^{(j)}} - \frac{1}{F_{0,T}^{(j)}}\right)\left(F_{t_i,T}^{(j)} - F_{t_{i-1},T}^{(j)}\right). \tag{18}$$

$$RP_T^{(j)} = OP_T^{(j)} + DS_T^{(j)}. \tag{19}$$

$$sBqv_T^{(j)} = \sqrt{Bqv_T^{(j)}\frac{1}{T}} \times 100 \tag{20}$$

$$sRP_T^{(j)} = \sqrt{RP_T^{(j)}\frac{1}{T}} \times 100 \tag{21}$$

$$e^{(j)} = sRP_T^{(j)} - sBqv_T^{(j)}. \tag{22}$$

$$\epsilon^{(j)} = \frac{sRP_T^{(j)} - sBqv_T^{(j)}}{sBqv_T^{(j)}}. \tag{23}$$

$$\text{RRMSE}^{(j)} = \sqrt{\frac{1}{n}\sum_{j=1}^{n}\left(\epsilon^{(j)}\right)^2}. \tag{24}$$

To assess the effectiveness of replicating our simulated strategy, we propose a series of test scenarios. As explained in Section 3.2.2, two error sources affect the evaluation of the options portfolio OP_T. The first relates to the increment in strike distance, denoted as ΔK_i. The second involves the truncation error of the OP_T integral. Variations in the lower and upper bounds of the integral directly influence the payoff of OP_T within the tails.

We employ various testing scenarios to tackle the first concern by adjusting the increment scale ΔK_i. We propose strategies, each representing a discretization scale of OP_T with $\Delta K_i = \{8, 15, 45\}$. These strike values will provide valuable insights into the behavior of integration in diverse market settings, particularly concerning the distance between the strikes. The value $\Delta K_i = 8$ represents the average increment observed on the date January 2, 2020, for the one-month maturity.

In this preliminary examination, we operate under the assumption of no truncation error in the evaluation of OP_T. To mitigate potential numerical instability, we set the lower bound as $K_1 = F_{0,T} - 3000$, ensuring a minimum moneyness of 0.0791. For the upper limit, we define $K_N = F_{0,T} + 3000$, resulting in a maximum moneyness of 1.9209. Additionally, we approximate the continuous scenario using a constant strike increment $\Delta K_i = 10^{-4}$.

Table 3: Descriptive statistics of ϵ in % and RRMSE for the Monte-Carlo Simulation concerning the discretization scale

Discretization scale	Min.	Median	Mean	Max.	SD	Quantile (95%)	RRMSE
Continuous	-0.0017%	0.0006%	0.0011%	0.2012%	0.0096%	0.0001%	0
$\Delta K_i = 8$	-13.9627%	-0.6971%	-1.3476%	0.0306%	1.6368%	-4.9772%	0.0212
$\Delta K_i = 15$	-28.2542%	-0.7059%	-2.2033%	0.1914%	3.2262%	-9.4191%	0.0390
$\Delta K_i = 45$	-81.4669%	-0.2327%	-3.6650%	1.9686%	6.9482%	-19.047%	0.0786

Descriptive statistics are provided for the relative replication error ϵ, defined as $\epsilon = \left(\frac{sRP_T - sBqv_T}{sBqv_T}\right)$, along with the computation of RRMSE for each discretization scale ΔK_i. Additionally, the analysis includes other metrics such as the minimum (Min), maximum (Max), 95th percentile (Quantile 95%), and standard deviation (SD). The simulation encompasses 100,000 paths with a maturity of $T = \frac{30}{365}$. The parameters align with those presented in Table 2. Integral bounds are set as $K_1 = 257.55$ and $K_N = 6257.55$ for a future price value of $F_{0,T} = 3257.55$.

As evident from Table 3, the results align closely with the findings presented in Bondarenko's (2014) [6]. Departures from continuity arise when employing different strategies with varying strike discretization scales, causing a divergence of OP_T from the continuous scenario. A larger ΔK_i corresponds to a higher relative replication error ϵ and RRMSE, resulting from an increased gap between the theoretical value Bqv_T and the reproduced value RP_T.

Furthermore, Figure 8 illustrates the box plot of the replication errors. This box plot reveals a negatively skewed distribution for the discrete strategies. In contrast, for continuous replication, the distribution is centered around 0, aligning with the results from Table 3.

Figure 8: Box plot of the relative replication errors on different scales

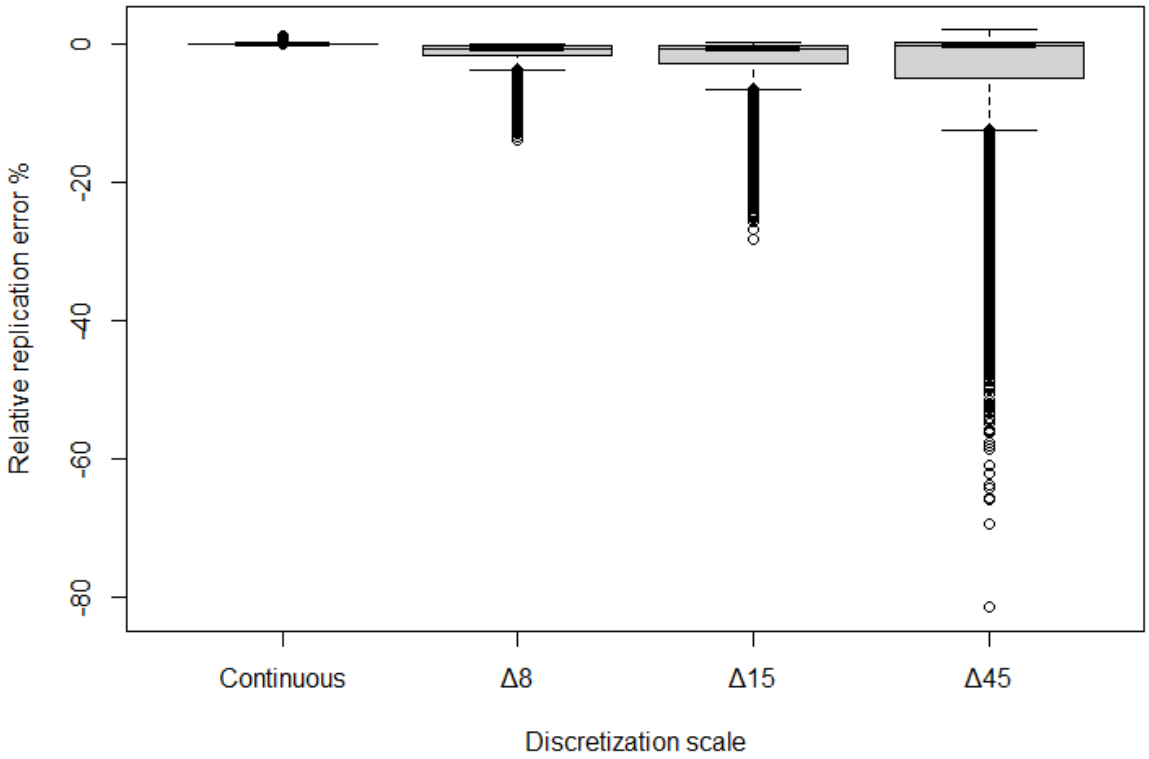

A box plot depicting the relative replication error ϵ across various discretization scales in a simulation involving 100,000 paths. The maturity is set at $T = 30/365$, and the parameters in use are taken from Table 2.

To address the second issue related to the truncation error, we conducted additional tests by adjusting the lower bound (LB) for the put parts integration of OP_T in Equation (13) and the upper bound (UB) for the call part of OP_T in Equation (14). In theory, these bounds are 0 and ∞, respectively, as mentioned in Section 3.2.2. However, in practical market scenarios, these strikes are not traded, which could potentially impact the payoff of OP_T. We propose three alternative strategies, each representing different truncation error level of OP_T. To simplify, we recommend maintaining a consistent gap between $F_{0,T}$[2] and the relevant bounds. For the put options, in term of the moneyness we suggest $LB = \{0.9463, 0.8465\}$[3], and for the call options, $UB = \{1.0537, 1.1535\}$[4]. In addition, at the initiation of our simulations on 2020-01-02, we take into account a market-like lower (puts) and upper (calls) bounds moneyness $\{0.78279, 1.0590\}$[5], taken from the real strike grid.

Table 4: Descriptive statistics for ϵ and RRMSE in the Monte Carlo Simulation concerning the truncation error.

Truncation error (moneyness bounds)	Min.	Median	Mean	Max.	SD	Quantile (95%)	RRMSE
None $\{0.0791, 1.9209\}$	-0.0026%	0.0006%	0.0009%	0.8976%	0.0069%	0.0001%	0
Medium $\{0.8465, 1.1535\}$	-2.2416%	0.0005%	0.0007%	0.3658%	0.0154%	0.0001%	0.0001
High $\{0.9463, 1.0537\}$	-98.6084%	0.0003%	-3.4644%	0.7419%	10.7573%	-24.0420%	0.1130
Market-like $\{0.7828, 1.0590\}$	-98.9086%	-0.7896%	-8.8482%	0.0331%	15.7784%	-45.9762%	0.1809

Descriptive statistics for the relative replication error ϵ defined as $\epsilon = \left(\frac{sRP_T - sBqv_T}{sBqv_T}\right)$ and the computation of RRMSE for every integration bound gap. The other metrics are respectively the minimum (Min), maximum (Max), Quantile (95%), and standard deviation (SD). The simulation is on 100,000 paths. The maturity is $T = 30/365$. The parameters are those of Table 2.

The results presented in Table 4 indicate that the higher the truncation error, the greater the relative replication error ϵ and RRMSE will be. Intuitively, this gap directly influences the outcomes of the static portfolio OP_T; potential payoffs resulting from large movements in the futures contract will not be captured if these moneyness bounds are not sufficiently far from 1. In the case of positive jumps, the call's payoff of the replication portfolio RP_T will be lower than Bqv_T if the upper bound moneyness UB is not significantly greater than 1. Analogously, in the case of negative jumps, the put's payoff of RP_T will be lower than Bqv_T if the lower bound moneyness LB is not sufficiently close to 0.

In the case of market-like truncation, we observe a significantly higher replication error. Notably, there is an asymmetry in terms of the bounds on each side. The left side of the truncation, which refers to the integration of the put payoffs, has a moneyness of 0.7828. In contrast, the right side of the truncation, related to the call payoffs, has a moneyness of only 1.0590. This asymmetry directly impacts the terminal payoff, OP_T, by undervaluing the call's payoff in the case of a positive jump.

Additionally, Figure 9 depicts the box plot of the replication errors. This box plot reveals a negatively skewed distribution as the truncation error increases. In contrast, the distribution is centered around 0 for continuous integration, consistent with the findings from Table 4.

[2]The suggested gap is chosen based on the level of the futures price $F_{0,T} = 3257.75$.
[3]Those moneyness are obtained by considering $LB = \{F_{0,T} - 175, F_{0,T} - 500\}$.
[4]Those moneyness are obtained by considering $UB = \{F_{0,T} + 175, F_{0,T} + 500\}$.
[5]Those moneyness are obtained by considering $LB = 2550$ and $UB = 3450$.

Figure 9: Box plot of the relative replication errors on different integration bounds gaps

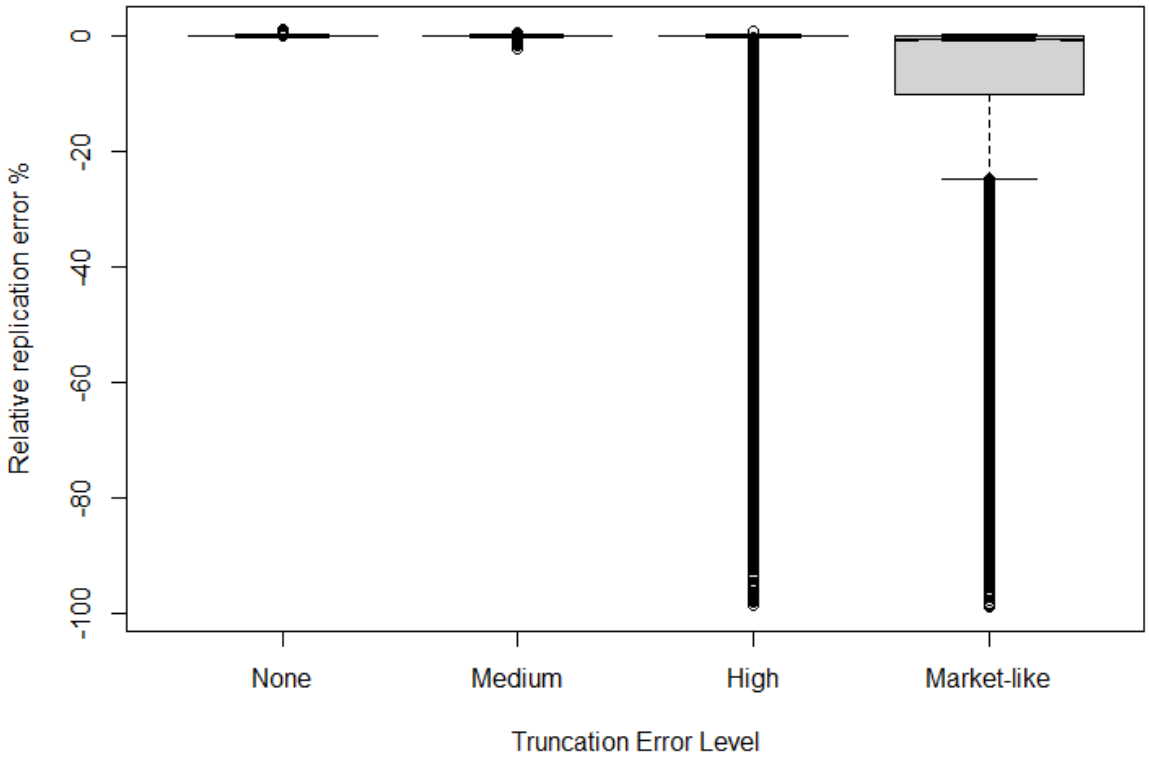

A box plot depicting the relative replication error ϵ across various truncation error levels in a simulation involving 100,000 paths. The maturity is set at $T = 30/365$, and the parameters in use are taken from Table 2.

3.2.4 Additional testings

To conclude our simulation testing, we conduct further analyses to identify the primary sources of error in evaluating Equation (15). This involves exploring the relative contributions of errors from both discretization scale and the truncation.

To evaluate this test, we examine simulated scenarios in which we simultaneously adjust both sources of errors and calculate their respective RRMSE metrics.

Table 5: RRMSE of the interaction of the two Integration error sources

Discretization scale/Truncation Error	None	Market-like	Medium	High
Continuous	0	0.1809	0.0001	0.1130
$\Delta K_i = 8$	0.0212	0.6113	0.6051	0.6058
$\Delta K_i = 15$	0.0390	0.6177	0.6120	0.6129
$\Delta K_i = 45$	0.0786	0.6150	0.6098	0.6131

Results of the RRMSE metric for each testing, where we simultaneously vary the discretization scale and the truncation error in estimating Equation (17), using 100,000 paths and the parameters specified in Table 2.

As shown in Table 5, when one factor of error is considered while keeping the other constant, the truncation error proves to be more dominant in terms of replication error than the discretization scale. Intuitively, the truncation plays a crucial role in capturing potential extreme payoffs, impacting the payoff of OP_T more than the discretization scale in the case of jumps in the underlying asset.

Examining the market-like grid indicates a substantially higher relative replication error RRMSE compared to hypothetical scenarios. Table 4 demonstrates that the imbalance in the truncation's bounds undervalues potential call option payoffs during positive jumps. Conversely, for negative jumps, OP_T is more apt to capture them, attributed to a moneyness of 0.7828 for the lower bound LB, lower than what is considered in medium and high truncation error scenarios.

3.3 Empirical study

In this section, we delve into various aspects related to applying real data in replicating the payoff Bqv_T. We initiate the discussion with an presentation of the data. Following that, we explore the implementation methodology and provide a numerical example. The empirical replication results are displayed across various maturities, spanning one, three, six months, and one year. Subsequently, we conduct an empirical analysis on the relative replication errors using regression analysis.

3.3.1 Implementation methodology

3.3.1.1 Rollover restrictions

The re-initialization phase of the strategies is driven by the expiration days of the futures and European options. This involves restrictions for the flexibility of the implementation of our rollover for the different maturities. To address this limitation, we adhere to a rule that allows us to practice the closest achievable rollover across various maturities.

For example, let's consider a 30-day replication strategy, taking our starting date as 2008-08-18. The futures and options available for this day expire on 2008-09-20. Therefore, the number of days for replication is 33. The issue is that on 2008-09-20, we may not find traded futures and options with approximately a 30-day maturity. To address this limitation, we must identify the closest trading day that offers an equivalent expiration time. In the case of our example, this date is 2008-09-22. Consequently, we need to repeat the same process. The next available contracts expire on 2008-10-18, resulting in a replication period of 26 days. Following this expiry date, our next rollover day is 2008-10-20.

Finally, we extend this methodology to all other horizons. We implement a single replication strategy for each unique combination of starting and expiring dates. Note that for a given time horizon, there is no overlap in time.

Table 6: Sub-sample of the characteristics of the contracts for rollover on different maturities

Maturity	Starting Date ($F_{0,T}$)	Expiration Date ($F_{t,T}$)	Number of Days	OTM Calls at t_0	OTM Puts at t_0
Monthly	2008-08-18	2008-09-20	33	29	44
Monthly	2008-09-22	2008-10-18	26	44	52
Monthly	2008-10-20	2008-11-22	33	48	80
Quarters	2019-11-15	2020-02-21	98	108	382
Quarters	2020-02-21	2020-05-15	84	148	460
Quarters	2020-05-15	2020-08-21	98	130	290
Semi-annual	2013-12-23	2014-06-21	180	12	39
Semi-annual	2014-06-23	2014-12-20	180	14	40
Semi-annual	2014-12-22	2015-06-19	179	11	49
Annual	2010-01-04	2010-12-31	361	10	13
Annual	2011-01-03	2011-12-30	361	9	11
Annual	2012-01-03	2012-12-31	363	14	26

Presentation of a sub-sample of consecutive rollover computations with their respective starting date, expiration date, number of days and quantity of OTM options since inception.

As shown in Table 6, an initial examination of our sample highlights the uneven distribution of futures and options availability across various expiration dates. The time remaining until expiration is approximately 1 month, 3 months, 6 months, and 1 year, with slight variations persisting over time.

3.3.1.2 Replication implementation

The implementation of the replication portfolio RP_T relies on the same methodology as Section 3. There are two main differences between the implementation. The first one involves the initial and terminal future price $F_{0,T}$ and $F_{t,T}$. We take those prices from real data according to entry and expiring dates selected by the methodology of 3.3.1.1. The second one is the distance between the strike prices ΔK.

At the initiation of the contract $t_0 = 0$, we adapt Equations (13) and (14) by taking all the available market's strike prices K^m. The strike distance ΔK^m is therefore not necessarily equidistant. This increment is directly affected by the contracts available at t_0. Note that the superscript m denotes the market's strikes to contrast with those of subsection 3.2.2.

We evaluate the payoff of the portfolio OP_T by considering the market grid with M options.

For $K_1^m < ... < K_{k-1}^m < F_{0,T} < K_k^m < ... < K_M^m$[6] ,

$$OP_T = 2\left\{\sum_{i=1}^{k-1} \frac{1}{2}\frac{\Delta K_i^m}{(K_i^m)^2}(K_i^m - F_{t,T})^+ + \sum_{i=k}^{M} \frac{1}{2}\frac{\Delta K_i^m}{(K_i^m)^2}(F_{t,T} - K_i^m)^+\right\}, \tag{25}$$

where $\Delta K_i^m = K_{i+1}^m - K_{i-1}^m$ for $2 \leq i \leq M-1$, $\Delta K_1^m = K_2^m - K_1^m$ and $\Delta K_M^m = K_M^m - K_{M-1}^m$.

On the other hand, the execution of the dynamic strategy DS_T remains unaffected. The strategy rebalances $\left(\frac{1}{F_{t_{i-1},T}} - \frac{1}{F_{0,T}}\right)$ shares every day t, tracking the empirical trajectory of the future from $F_{0,T}$ to $F_{t,T}$. This rebalancing occurs on a daily frequency for both short-term and long-term maturities.

Finally, we apply the same scaling that is performed in Equations (20) and (21).

[6]Note the necessity for a correction if $K_{k-1}^m \leq F_{0,T}$ as presented in subsection 3.2.2.

3.3.2 Numerical example

To provide clarity to our replication implementation, let's examine the following numerical example. We consider the monthly replication during the COVID-19 crisis. The starting date is 2020-03-04 and the expiration date is 2020-04-03. The maturity $T = 30/365$, the initial future price $F_{0,T} = 3129.15$ and the terminal one $F_{t,T} = 2541.77$.

The replication result for our example is presented in Table 7. This particular example precisely captures a financial crisis, with the index losing 20.79%. Consequently, all the calls in OP_T expired worthless, and out of the 156 puts purchased at t_0, 117 ended in-the-money at expiration date. Figure 10 shows the future price evolution during our example's reference period.

Table 7: Results of the replication of Bqv_T payoff for the numerical example

Starting Date	Expiration Date	$F_{0,T}$	$F_{t,T}$	Bqv_T	RP_T	OP_T	DS_T	$sBqv_T$	sRP_T	ϵ
2020-03-04	2020-04-03	3129.15	2541.77	0.0683	0.0678	0.0399	0.0279	91.1582	90.8240	-0.3666%

Table containing the results of the numerical example computing the replication portfolio RP_T for the COVID-19 crisis from March 4, 2020, to April 3, 2020. $F_{0,T}$ and $F_{t,T}$ represent the futures prices at the starting and expiration dates, respectively. Bqv_T denotes Bondarenko's quadratic variation value. OP_T is the static portfolio payoff for the period. DS_T is the value of the dynamic trading strategy at T. $sBqv_T$ is the scaled transformation for Bqv_T. sRP_T is the scaled transformation of RP_T and ϵ is the relative error between sRP_T and $sBqv_T$.

Figure 10: Time series of the futures price for the numerical example.

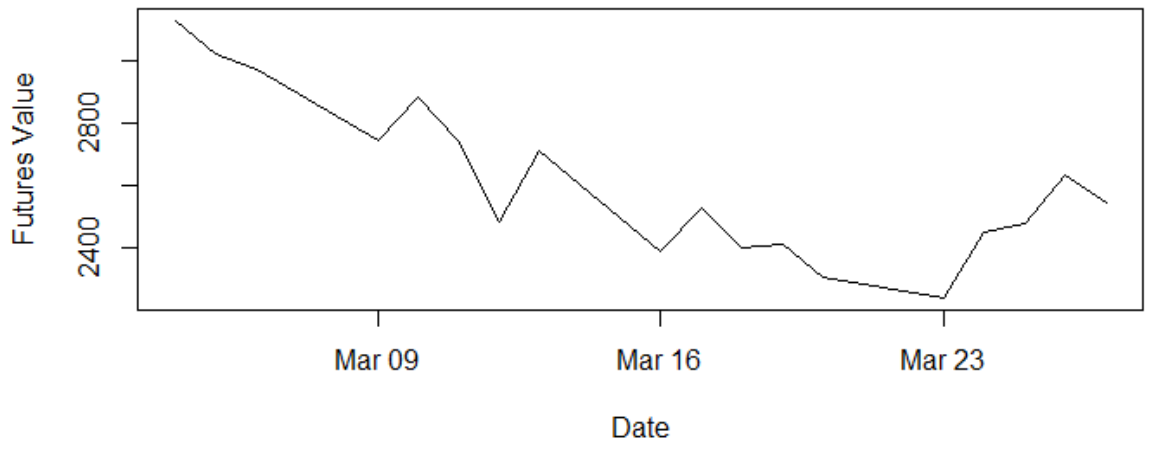

Time series of the future price for the numerical example during the COVID-19 crisis period from March 4, 2020, to April 3, 2020.

The first step is to calculate the Bqv_T payoff with the application of Equation (16) but taking into account our example's trajectory of the future from $F_{0,T}$ to $F_{t,T}$.

The second step is to take into consideration the strike prices at $t_0 = 0$. For the puts grid, the moneyness domain is $[0.5113, 0.9987]$[7] with a ΔK^m average of 9.58 and a number of 156 puts. For the calls grid, the moneyness domain is $[1.0002, 1.1585]$[8] with a ΔK^m average of 5 and a number of 100 calls.

The third step is to compute OP_T using the inputs of the second step and Equation (25). The strike distance ΔK_i^m and the portfolio's weights $1/\left(K_i^m\right)^2$ are obtained explicitly from the observed strike prices grid. The next step is to evaluate OP_T by taking into consideration the terminal futures price $F_{t,T}$ to obtain the portfolio's payoff at T.

The fourth step is to compute the dynamical strategy DS_T with the application of Equation (18) but taking in the case of our example's trajectory of the future from $F_{0,T}$ to $F_{t,T}$.

Finally, the last step is to obtain our replication portfolio RP_T by simply adding the results of the third step and fourth step. We then apply the scaled transformation of Equations (20) and (21) to obtain $sBqv_T$ and sRP_T.

3.3.3 Empirical trading results

As we implement the trading strategy outlined in Subsection 3.3.1, differences arise between the scaled theoretical target $sBqv_T$ and the value of the scaled replication portfolio sRP_T. To delve deeper into these disparities, we employ the error metrics defined from Equations (19) to (24) in Section 3.2.3.

Table 8: Descriptive statistics of the relative error for the Empirical replication

Maturity	Min.	Median	Mean	Max.	SD	Quantile (95%)	RRMSE	Strategies
Monthly	-44.8338%	-0.9344%	-2.1294%	2.2551%	3.6480%	-7.8979%	0.0422	777
Quarters	-52.7025%	-0.7940%	-2.6418%	30.0325%	7.0301%	-11.6456%	0.0748	156
Semi-annual	-30.8768%	-1.0141%	-2.6697%	28.0913%	6.0364%	-13.8805%	0.0657	112
Annual	-25.1782%	-0.8572%	-2.5534%	10.9645%	4.7307%	-11.1102%	0.0535	85

Descriptive statistics of the relative error ϵ for the replication, defined in percentage as $100 \times \left(\frac{sRP_T - sBqv_T}{sBqv_T}\right)$. The metrics are respectively the minimum (Min), maximum (Max), Quantile (95%), and the number of strategies.

In Table 8, the outcomes related to ϵ in the real data reflect the effective performance of the strategies. Initially, we observe a consistently low replication gap of -3% across all maturities on average. Additionally, the relatively low value of the RRMSE indicates a generally strong replication performance.

The panels in Figure 11 display the successful replication of the payoff across various maturities. Both short and long-term strategies successfully capture the spike in volatility, primarily linked to financial turmoil. Furthermore, Figure 12 presents the time series of ϵ over time. In the high volatility period corresponding to the financial crisis (grey shadow), ϵ is impacted only at the beginning of the one-year rollover during the Asian crisis of 1997.

[7] This range is obtained with a strike grid of $[1600, 3125]$ for the puts.
[8] This range is obtained with a strike grid of $[3130, 3625]$ for the calls.

Figure 11: Time series of the empirical replication for different maturities.

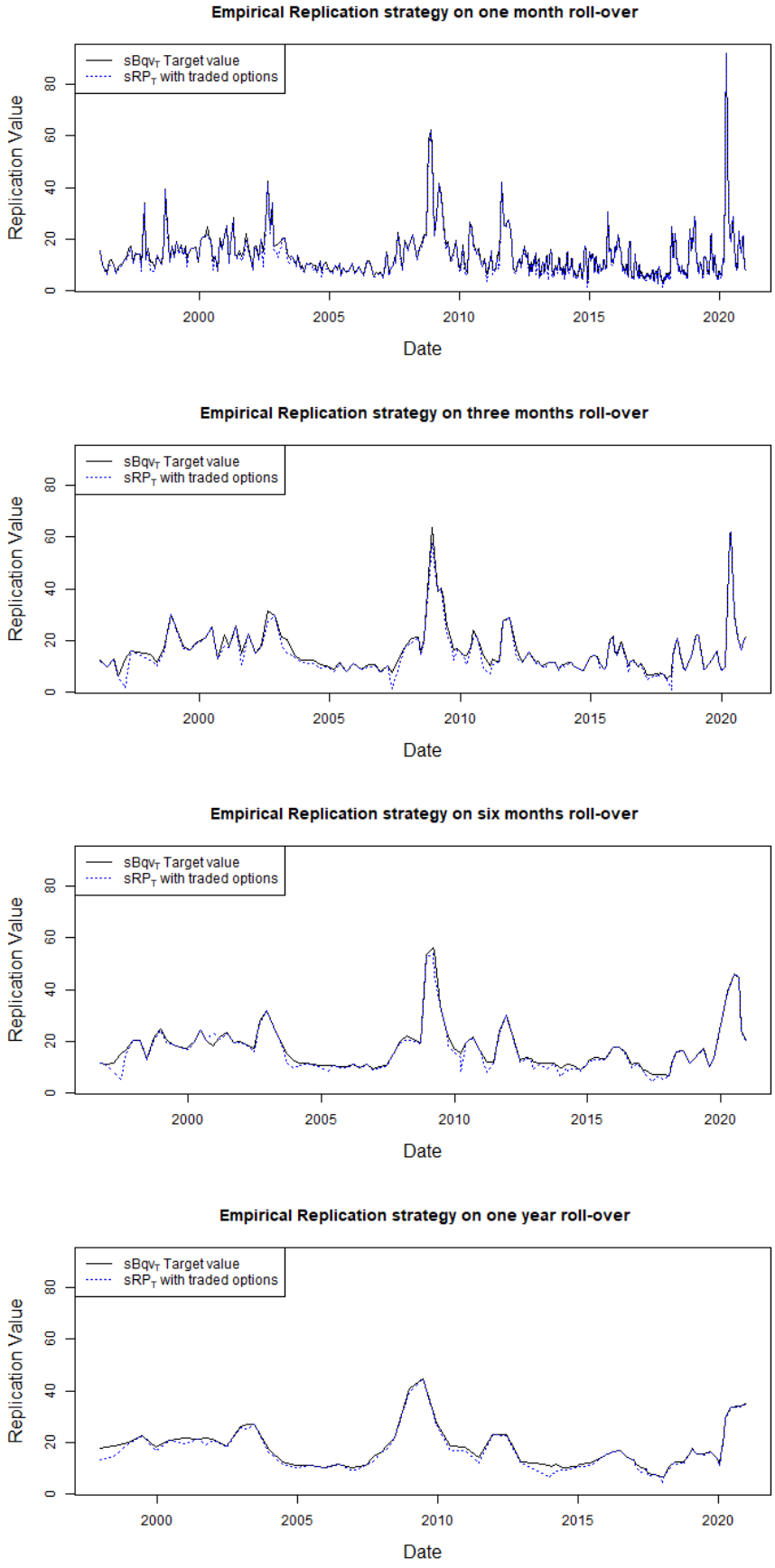

Panel showing the comparison on the different maturities between the scaled empirical replication sRP_T and the target value $sBqv_T$.

Figure 12: Panel of the relative error of the replication for different maturities.

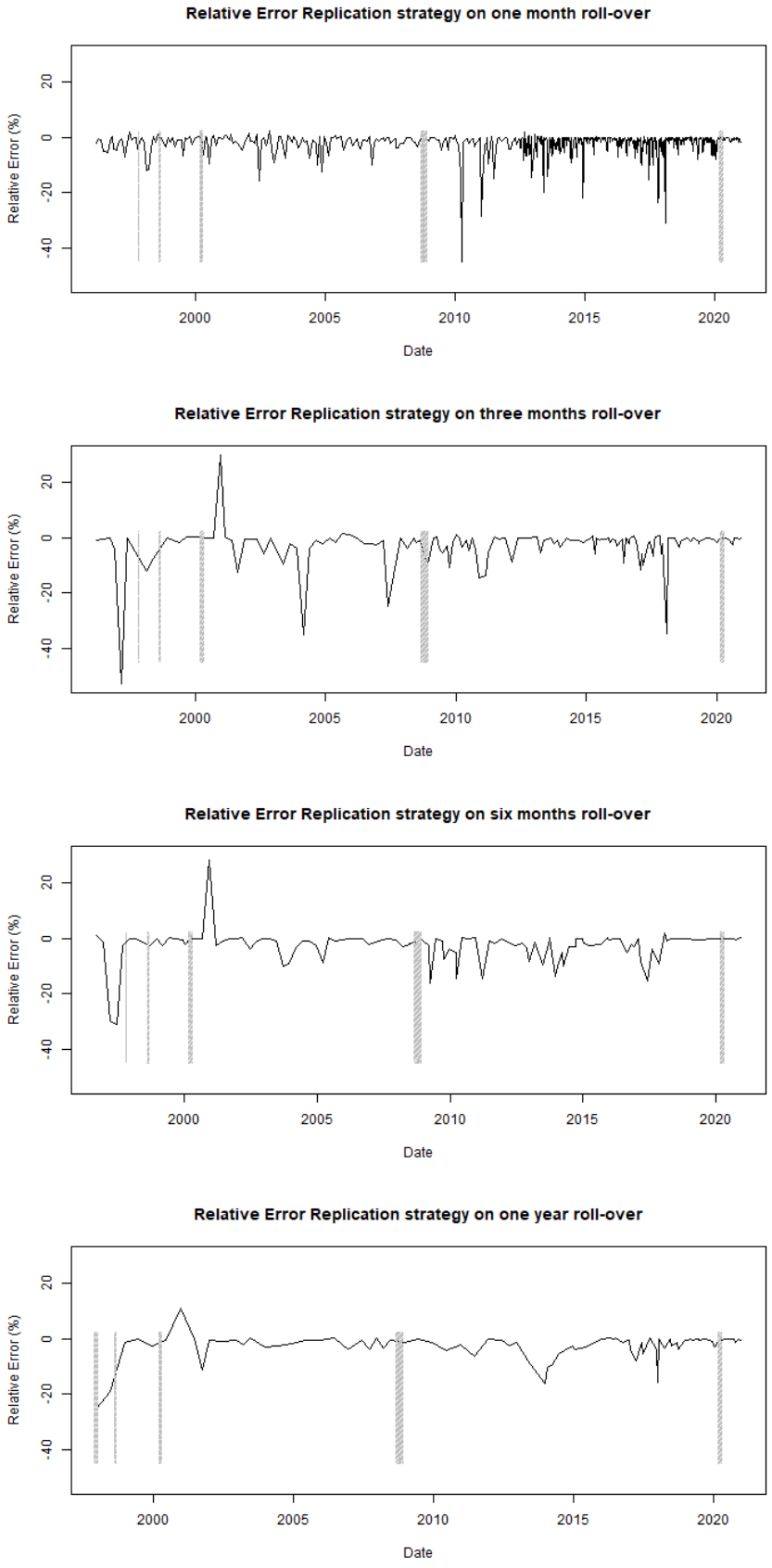

Panel showing the relative error of the replication ϵ on the different maturities, defined in percentage of the scaled payoffs as $100 \times \left(\frac{sRP_T - sBqv_T}{sBqv_T} \right)$. With grey shadow emphasizes the Asian (1997) and Russian crises (1998), the dot-com bubble (2000), the global financial crisis (2008), and the COVID-19 pandemic (2020).

Additionally, we can establish a connection between the truncation error and the moneyness of the deepest options available on the left and right sides of the volatility surface. For calls, the upper bound moneyness is calculated by taking the ratio of the maximum strike $K^{max} = K_M^m$ available on each contract inception day t_0 to the current $F_{0,T}$. Similarly, for puts, the lower bound moneyness is determined by considering the minimum strike $K^{min} = K_1^m$ divided by the current future prices.

Figures 13 and 14 depict a time series for the option moneyness at t_0. Additionally, Tables 9 and 10 present the descriptive statistics for these figures.

Figure 13: Time series of the moneyness of the market's call options

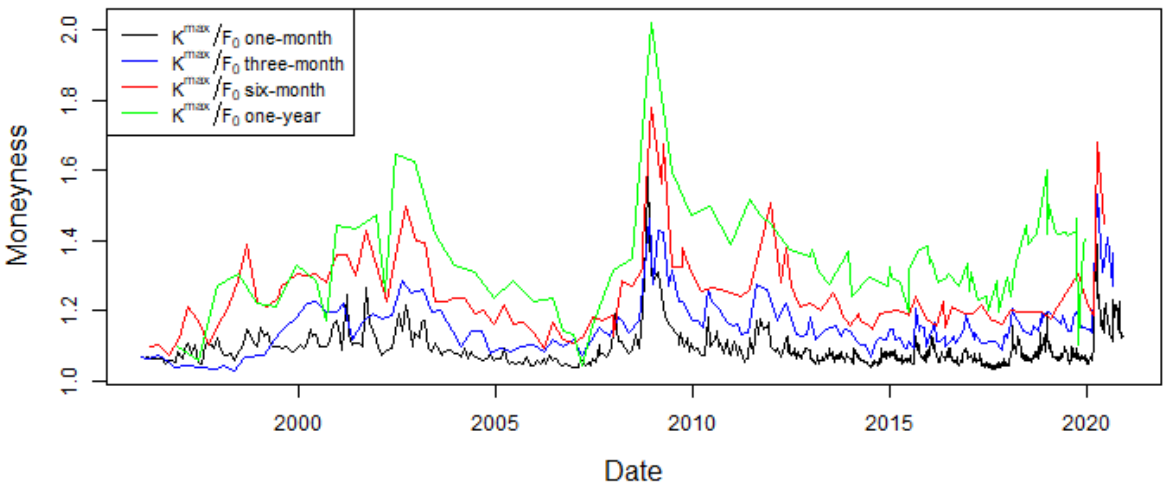

Time series of the moneyness of calls obtained for the maximum strike K^{max}, calculated by dividing it by the initial future prices $F_{0,T}$ across all maturities.

Figure 14: Time series of the moneyness of the market's put options

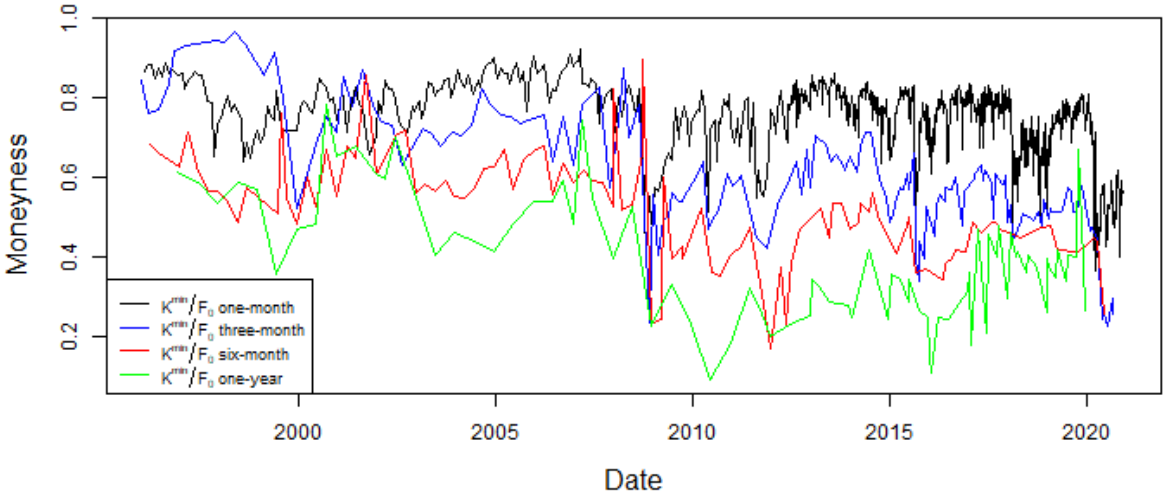

Time series of the moneyness of the puts obtained for the minimum strike K^{min}, calculated by dividing it by the initial future prices $F_{0,T}$ across all maturities.

Table 9: Descriptive statistics of the maximum strike moneyness

Maturity	Min.	1st Qu.	Median	Mean	3rd Qu.	Max.	Strategies
Monthly	1.032	1.059	1.072	1.087	1.095	1.588	777
Quarterly	1.029	1.113	1.145	1.161	1.189	1.535	156
Semi-annual	1.073	1.178	1.216	1.250	1.290	1.777	112
Annual	1.045	1.258	1.326	1.339	1.418	2.023	85

Descriptive statistics of the maximum strike moneyness. The metrics are respectively the minimum (Min), maximum (Max), first quantile (1st Qu.),third quantile (3rd Qu.) and the number of strategies on each maturity.

Table 10: Descriptive statistics of the minimum strike moneyness

Maturity	Min.	1st Qu.	Median	Mean	3rd Qu.	Max.	Strategies
Monthly	0.3633	0.7061	0.7707	0.7440	0.8052	0.9216	777
Quarterly	0.2244	0.5130	0.5871	0.6067	0.7082	0.9660	156
Semi-annual	0.1674	0.4466	0.5219	0.5193	0.5926	0.8935	112
Annual	0.0908	0.2793	0.3874	0.3932	0.4805	0.7825	85

Descriptive statistics of the minimum strike moneyness. The metrics are respectively the minimum (Min), maximum (Max), first quantile (1st Qu.),third quantile (3rd Qu.) and the number of strategies on each maturity.

3.3.4 Regression analysis of the relative error

In this section, we will examine potential sources of replication errors in our strategies. To address this, we will conduct a regression analysis on the relative replication error, denoted as ϵ. This statistical study aims to be inferential rather than an attempt at forecasting. This focus is primarily due to the fact that the relative error ϵ is computed at time T and is driven by current and future variables.

Therefore, the response variable is denoted as ϵ. The selection of explanatory variables is informed by the diverse factors examined in Section 3. The first explanatory variable, *contracts*, represents the total quantity of calls and puts available at the contract's inception date t_0. Secondly, to address the truncation error in the integral of the static portfolio, we also consider the minimum and maximum moneyness ratios: $\frac{K^{min}}{F_{0,T}}$ and $\frac{K^{max}}{F_{0,T}}$. Additionally, to account for periods of high volatility, especially during financial turbulence, we include the 30-day at-the-money (ATM) implied volatility at the expiration date T. Finally, we incorporate the logarithm of the return of the futures contract, $\ln\left(\frac{F_{t,T}}{F_{0,T}}\right)$, during the reference period.

After confirming the absence of collinearity[9], we estimate the regression model using the ordinary least squares (OLS) method without variable selection.

$$\epsilon = \beta_1 contracts + \beta_2 \frac{K^{min}}{F_{0,T}} + \beta_3 \frac{K^{max}}{F_{0,T}} + \beta_4 AtmIV_T + \beta_5 \ln\left(\frac{F_{t,T}}{F_{0,T}}\right) + error. \tag{26}$$

Table 11: Regression analysis without variable selection on all maturities

Variables	One-month	Three-month	Six-month	One-year
contracts	1.546e-05	1.526e-05	0.0001	0.0002
	(0.987)	(0.310)	(0.787)	(1.528)
$\frac{K^{min}}{F_{0,T}}$	-0.0727***	-0.1032**	-0.0666	-0.0733*
	(-4.911)	(-2.821)	(-1.535)	(-2.164)
$\frac{K^{max}}{F_{0,T}}$	0.0358*	0.0695*	0.0284	0.0158
	(2.460)	(2.192)	(0.962)	(0.972)
30-day $AtmIV_T$	-0.0324	-0.2013*	-0.1339	-0.1011·
	(-1.258)	(-2.087)	(-1.255)	(-1.744)
$\ln\left(\frac{F_{t,T}}{F_{0,T}}\right)$	-0.2103***	-0.3624***	-0.2004**	-0.1718***
	(-5.616)	(-3.978)	(-2.913)	(-4.377)
Degree of freedom	772	151	107	80
Adjusted-R^2	0.3118	0.2053	0.2021	0.3462
RSE	0.0350	0.0668	0.0587	0.0433

This table presents the summary of the OLS regression analysis for the relative error (ϵ) across the four different maturities. The t-test values of the estimators are shown in parentheses. The legend for the stars is as follows: *** (99.9%), ** (99%), * (95%), · (90%). The fitting quality is measured by the adjusted R-squared and the residual standard error RSE, accounting for the number of variables in each model.

[9]Refer to Appendix C for the correlations matrix.

The results presented in Table 11 a priori indicate good performance in explaining the relative errors ϵ in terms of the adjusted R-squared and the RSE. There is coherence in terms of the variables $\frac{K^{min}}{F_{0,T}}$ and $\frac{K^{max}}{F_{0,T}}$ capturing the truncation error.

However, there are issues with the coherence of the coefficients concerning the 30-day ATM implied volatility. Firstly, there is no statistical significance for the one-month horizon regression, which is not intuitively expected since the 30-day ATM should be the most sensitive for this maturity. Secondly, the coefficient for this explanatory variable is negative for all the maturities in Table 11, which is also not coherent with the correlation between $AtmIV_T$ and ϵ, varying from 0.0321 to 0.1615 according to our correlation matrix in Tables 18 to 21. Additionally, there is similarity in the coefficient sign between $AtmIV_T$ and $\ln\left(\frac{F_{t,T}}{F_{0,T}}\right)$ across all maturities, which is also not coherent with the correlation matrix, since the correlation between those variables varies from -0.4224 to -0.5897.

For all these reasons, we have decided to conduct various regression estimation with different selections of variables.

Considering the various possibilities of variable combinations, we select the top-performing six models for the in-sample one-month rollover based on their adjusted R-squared, residual standard error, economic interpretation, and statistical significance of coefficients[10]. We opt for the one-month sample due to its higher number of observations.

The interpretation of the sign for the estimators leads to intuition in the context of relative error. In fact, ϵ can have a negative value, indicating under-performance of RP_T, or a positive value, indicating over-performance of RP_T.

Table 12: Regression analysis for the one-month rollover

Variables	(1)	(2)	(3)	(4)	(5)	(6)
Number of contract			2.524e-05·		4.147e-05***	
			(1.915)		(3.342)	
$\frac{K^{min}}{F_{0,T}}$	-0.0615***	-0.0426***	-0.0441***	-0.0359***	-0.0340***	-0.0678***
	(-5.825)	(-11.15)	(-11.320)	(-8.940)	(-13.840)	(-6.541)
$\frac{K^{max}}{F_{0,T}}$	0.0225**					0.0278***
	(3.094)					(3.885)
30-day ATM IV		0.0557***	0.0471**	0.0324*		
		(3.89)	(3.150)	(2.163)		
$\ln\left(\frac{F_{t,T}}{F_{0,T}}\right)$				-0.1457***	-0.1735***	-0.1821***
				(-4.655)	(-5.895)	(-6.166)
Degree of freedom	775	775	774	774	774	774
Adjusted-R^2	0.2776	0.2827	0.2852	0.3013	0.3071	0.3106
RSE	0.0359	0.0358	0.0357	0.0353	0.0351	0.0350

This table presents the summary of the OLS regression analysis for the one-month rollover relative error (ϵ) across six different models. The t-test values of the estimators are shown in parentheses. The legend for the stars is as follows: *** (99.9%), ** (99%), * (95%), · (90%). The fitting quality is measured by the adjusted R-squared and the residual standard error RSE, accounting for the number of variables in each model.

[10]We perform model selection through an exhaustive search using the regsubsets function from the R package leaps.

In Table 12, for the one-month horizon, we observe the impact on the different explanatory variables selected. We begin by analyzing the regression results for the variables studied in Section 3.3.4. The total number of contracts has a mild impact on the relative error ϵ; as the number of contracts increases, the replication tends to shift towards the positive area (over-replicating). This impact is relatively small in the models that includes these variables.

For the truncation error, we can see that $\frac{K^{min}}{F_{0,T}}$ has a significant effect on the replication performance. A rise in this metric corresponds to an elevation in the left-side truncation error of OP_T's integral, resulting in under-replication. Analogously, for $\frac{K^{min}}{F_{0,T}}$, we observe that an increase in this metric results in a reduction in the right-side truncation error, leading to a shift of ϵ in the positive area.

However, upon examining the coefficient estimations, it becomes apparent that the maximum moneyness appears to be 30 to 45% less impactful than the coefficients for the minimum moneyness. This observation could be explained by the composition of our sample, which is predominantly constituted of puts, as demonstrated in Table 1.

Regarding the 30-day At-The-Money (ATM) implied volatility, we observe a significant and positive impact on our replication performance. This means that when the 30-day ATM implied volatility spikes, our replication strategy shows improved performance, with the relative error shifting towards the positive area.

Furthermore, we observe a substantial and statistically significant influence of the log return during the contract's reference period (from t_0 to T) on our replication strategy's performance. During periods of growth, the replication performance experiences considerable under-performance. Conversely, in periods of significant decline, the replication over-performs. It's worth noting that in Model (4) of Table 12, an inverse relationship is evident between the log return and the At-The-Money (ATM) 30-day implied volatility.

Additionally, we observe that the performance of Model (4) closely resembles that of the regression without variable selection in Table 11. The primary distinction lies in the economic interpretation, which is more intuitive due to the contrast in the signs of $AtmIV_T$ and $\ln\left(\frac{F_{t,T}}{F_{0,T}}\right)$, as well as its coherence with the correlation matrix.

Finally, upon an overall evaluation of our regression analysis for the one-month rollover, we observe well-performing models in terms of the adjusted R-squared and RSE. The variables with the most significant impact are the minimum moneyness $\frac{K^{min}}{F_{0,T}}$ and the log return $\ln\left(\frac{F_{t,T}}{F_{0,T}}\right)$.

Table 13: Regression analysis for the three-month rollover

Variables	(1)	(2)	(3)	(4)	(5)	(6)
Number of contract			4.599e-05		6.692e-05	
			(1.108)		(1.716)	
$\frac{K^{min}}{F_{0,T}}$	-0.0700*	-0.0564**	-0.0570**	-0.0386·	-0.0494***	-0.0945**
	(-2.192)	(-2.733)	(-2.762)	(-1.831)	(-4.809)	(-2.979)
$\frac{K^{max}}{F_{0,T}}$	0.0139					0.0307·
	(0.813)					(1.779)
30-day ATM IV		0.0379	0.0182	-0.0055		
		(0.611)	(0.282)	(-0.089)		
$\ln\left(\frac{F_{t,T}}{F_{0,T}}\right)$				-0.2172**	-0.2330**	-0.2535***
				(-2.924)	(-3.229)	(-3.402)
Degree of freedom	154	154	153	153	153	153
Adjusted-R^2	0.1338	0.1321	0.1334	0.1727	0.1883	0.1894
RSE	0.0697	0.0698	0.0697	0.0681	0.0675	0.0674

This table presents the summary of the OLS regression analysis for the three-month rollover relative error ϵ across six different models. The t-test values of the estimators are shown in parentheses. The legend for the stars is as follows: *** (99.9%), ** (99%), * (95%), · (90%). The fitting quality is measured by the adjusted R-squared and the residual standard error RSE, accounting for the number of variables in each model.

For Table 13, we observe a consistent impact for the minimum moneyness $\frac{K^{min}}{F_{0,T}}$ and the log returns, similar to the one-month rollover. However, there is a notable contrast in the impacts of the ATM 30-day implied volatility and the maximum moneyness $\frac{K^{max}}{F_{0,T}}$, which are not statistically significant. By referring to Figure 13 and Table 9, and comparing the time series of the one-month versus the three-month rollovers, we notice a higher average $\frac{K^{max}}{F_{0,T}}$ and lower volatility clustering during high turbulence periods.

In summary, the models provide an overall good quality in explaining the replication gaps for the three-month rollover, considering the selected in-sample criteria from the one-month rollover. The adjusted R-squared ranges from 0.1338 to 0.1894, and the RSE ranges from 0.0675 to 0.0698.

Table 14: Regression analysis for the six-month rollover

Variables	(1)	(2)	(3)	(4)	(5)	(6)
Number of contract			2.826e-05		0.0001	
			(0.175)		(0.955)	
$\frac{K^{min}}{F_{0,T}}$	-0.0364	-0.0665*	-0.0665*	-0.0399	-0.0553***	-0.0728·
	(-0.930)	(-2.416)	(-2.405)	(-1.400)	(-3.675)	(-1.818)
$\frac{K^{max}}{F_{0,T}}$	-0.0059					0.0125
	(-0.355)					(0.719)
30-day ATM IV		0.0435	0.0377	-0.0131		
		(0.656)	(0.508)	(-0.194)		
$\ln\left(\frac{F_{t,T}}{F_{0,T}}\right)$				-0.1344**	-0.1392**	-0.1449**
				(-2.712)	(-2.921)	(-2.862)
Degree of freedom	110	110	109	109	109	109
Adjusted-R^2	0.15	0.1523	0.1448	0.1986	0.205	0.2021
RSE	0.0606	0.0605	0.0608	0.0588	0.0586	0.0587

This table presents the summary of the OLS regression analysis for the six-month rollover relative error ϵ across six different models. The t-test values of the estimators are shown in parentheses. The legend for the stars is as follows: *** (99.9%), ** (99%), * (95%), · (90%). The fitting quality is measured by the adjusted R-squared and the residual standard error RSE, accounting for the number of variables in each model.

For Table 14, the impact of $\frac{K^{min}}{F_{0,T}}$ and $\ln\left(\frac{F_{t,T}}{F_{0,T}}\right)$ remains significant, with Models (5) and (6) explaining the majority of ϵ. With a lower degree of freedom, the adjusted R-squared is higher than in the three-month rollover, ranging from 0.1448 to 0.205, and a lower RSE ranging from 0.0586 to 0.0608. Note that in this maturity, Model (5) performs slightly better than the regression without variable selection in Table 11.

Table 15: Regression analysis for the one-year rollover

Variables	(1)	(2)	(3)	(4)	(5)	(6)
Number of contract			3.366e-05		0.0002*	
			(0.275)		(2.030)	
$\frac{K^{min}}{F_{0,T}}$	-0.0431	-0.0648*	-0.0659*	-0.0471·	-0.0761***	-0.0973**
	(-1.376)	(-2.477)	(-2.477)	(-1.893)	(-4.586)	(-3.047)
$\frac{K^{max}}{F_{0,T}}$	-0.0056					0.0161
	(-0.573)					(1.533)
30-day ATM IV		0.0109	0.0047	-0.0095		
		(0.224)	(0.088)	(-0.209)		
$\ln\left(\frac{F_{t,T}}{F_{0,T}}\right)$				-0.1105***	-0.1353***	-0.1373***
				(-3.659)	(-4.248)	(-3.968)
Degree of freedom	83	83	82	82	82	82
Adjusted-R^2	0.2035	0.2009	0.1919	0.3047	0.3376	0.3237
RSE	0.0477	0.0478	0.0481	0.0446	0.0436	0.0440

This table presents the summary of the OLS regression analysis for the one-year rollover relative error (ϵ) across six different models. The t-test values of the estimators are shown in parentheses. The legend for the stars is as follows: *** (99.9%), ** (99%), * (95%), · (90%). The fitting quality is measured by the adjusted R-squared and the residual standard error RSE, accounting for the number of variables in each model.

For Table 15, the impact of $\frac{K^{min}}{F_{0,T}}$ and $\ln\left(\frac{F_{t,T}}{F_{0,T}}\right)$ remains significant, with Models (5) and (6) explaining the majority of ϵ. In the case of the one-year rollover, these models provide a better explanation of the replication's relative performance. Given the longer horizon, the robustness of the chosen variables is evident in the quality of the fitting. The adjusted R-squared is higher than in the three and six-month rollovers, ranging from 0.1919 to 0.3047, with a lower RSE ranging from 0.0436 to 0.0481. Furthermore, Model (5) offers a performance similar to that of the regression in Table 11, but with more significant explanatory variables.

In summary of this section, the regression analysis demonstrates that the performance of our replication strategies relies mainly on three variables. The first one is the truncation error measured by the two minimum and maximum moneyness ratios, $\frac{K^{min}}{F_{0,T}}$ and $\frac{K^{max}}{F_{0,T}}$. The second one is the 30-day ATM IV. Finally, the third one is the log return of the contract's period (from t_0 to T).

4 Valuation of the risk-neutral contracts

In this section, we concentrate on the mark-to-market valuation of contracts, aiming to support financial agents considering purchase or writing these contracts at the inception date $t_0 = 0$. A comparative analysis of two valuation methods is conducted for a 30-day variance contract and the rare disaster index ($\mathbb{RIX}$). The classical trapezoidal technique is employed as the first method, while the second method use the volatility surface model.

4.1 Valuation methodology

For the variance contract, the dynamic part DS_T being a discrete position on the index futures contract, the discretization concerns strictly the static portfolio OP_T.

The valuation concern the Equation (8),

$$\mathbb{E}_0^{\mathbb{Q}}\left[e^{-rT}RP_T\right] = 2\left\{\int_0^{F_{0,T}} \frac{1}{K^2}P(F_{0,T},K,T)dK + \int_{F_{0,T}}^{\infty} \frac{1}{K^2}C(F_{0,T},K,T)dK\right\}.$$

For valuing $\mathbb{E}_0^{\mathbb{Q}}\left[e^{-rT}RP_T\right]$, we use the inception and expiration dates selected through the methodology in Section 3.3.1.

4.1.1 Trapezoidal method

The first method to evaluate Equation (8) is by approximating the integrals with the use of numerical techniques such as the trapezoidal rule present in Section 3.2.3

Recalling the notation of Section 3.3.1.2, at the initiation of the contract $t_0 = 0$, K^m represents the available market strike prices, where the superscript m denotes the market's strikes to contrast with those of subsection 3.2.2. Additionally, the strike distance ΔK^m is not equidistant. We adopt the same entry date for the monthly contracts as in Section 3.3. The sole distinction lies in the consideration of option prices here, as opposed to the terminal payoff at time T. We evaluate the value of the portfolio OP_T by considering the market grid with M options and adapting Equations (13) and (14) with the market's option prices $P(F_{0,T},K,T)$ and $C(F_{0,T},K,T)$.

For $K_1^m < ... < K_{k-1}^m < F_{0,T} < K_k^m < ... < K_M^m$[11],

$$\mathbb{E}_0^{\mathbb{Q}}\left[e^{-rT}RP_T\right] \cong 2\left\{\sum_{i=1}^{k-1}\frac{1}{2}\frac{\Delta K_i^m}{(K_i^m)^2}P(F_{0,T},K,T) + \sum_{i=k}^{M}\frac{1}{2}\frac{\Delta K_i^m}{(K_i^m)^2}C(F_{0,T},K,T)\right\}, \quad (27)$$

where $\Delta K_i^m = K_{i+1}^m - K_{i-1}^m$ for $2 \leq i \leq M-1$, $\Delta K_1^m = K_2^m - K_1^m$ and $\Delta K_M^m = K_M^m - K_{M-1}^m$.

[11] Note the necessity for a correction if $K_{k-1}^m \leq F_{0,T}$ as presented in subsection 3.2.2.

Additionally, we evaluate the $\mathbb{RIX}$ with the same grid but considering only the put's strikes

$$\mathbb{RIX} \cong \sum_{i=1}^{k-1} \frac{1}{2} \frac{\Delta K_i^m \ln\left(\frac{F_{0,T}}{K_i^m}\right)}{(K_i^m)^2} P(F_{0,T}, K, T). \tag{28}$$

Finally, we apply the identical scaling transformation for both contracts that we apply in Equations (20) and (21).

4.2 Valuation using the Volatility surface model

The second valuation method involves employing the implied volatility surface model of François et al. (2022) [22] as detailed in Appendix D. This approach helps assess $\mathbb{E}_0^{\mathbb{Q}}\left[e^{-rT} RP_T\right]$ across a wide spectrum of options prices. By employing the daily estimators, represented as $\{\beta_1, \beta_2, \beta_3, \beta_4, \beta_5\}$, one can effectively interpolate or extrapolate the implied volatility for each contract initiation date.

By the following IV surface fitting equations,

$$M = \frac{1}{\sqrt{T}} \ln\left(\frac{F_{t,T}}{K}\right). \tag{29}$$

$$\begin{aligned}\hat{\sigma}(M,T) = \beta_1 + \beta_2 \exp\left(-\sqrt{T/T_c}\right) + \beta_3 \left(M \mathbb{1}_{M \geqq 0} + \frac{e^{2M}-1}{e^{2M}+1} \mathbb{1}_{M<0}\right) \\ + \beta_4 \left(1 - \exp\left(-M^2\right)\right) \ln\left(T/T_m + \beta_5 (1 - \exp((3M)^3)) \ln(T/T_m) \mathbb{1}_{M<0},\right.\end{aligned} \tag{30}$$

where M is the moneyness, T is the time to maturity (365-day basis), $F_{t,T}$ the future price, and K is the strike price. β_1 captures the long-term at-the-money implied volatility level, β_2 the time to maturity slope, β_3 the moneyness slope, β_4 the smile attenuation and β_5 the smirk. In addition, the model relates to two fixed values, T_m as the extrapolation proxy of the longest time to maturity of the sample and T_c as the location of the fast convexity change in the IV term structure.

To conduct the interpolation and extrapolation of implied volatility, we establish the strike range as $[K_1^m - 20\%, K_M^m + 10\%]$. Within this continuous grid, we calculate the moneyness using Equation (29) and employ it in the model described by Equation (30) to obtain the implied volatility. Subsequently, this estimated implied volatility serves as an input in the Black model [5] to price the European options. Note that we consider only the options prices greater or equals to 0.01\$.

Recall the Black model main equation,

$$\begin{aligned} C(F_{0,T}, K, T)^{model} &= \exp(-rT)\left[F_{0,T}\Phi(D_1) - K\Phi(D_2)\right]. \\ P(F_{0,T}, K, T)^{model} &= \exp(-rT)\left[K\Phi(-D_2) - F_{0,T}\Phi(-D_1)\right]. \\ D_1 &= \frac{\ln(F_{0,T}/K) + \frac{1}{2}\hat{\sigma}^2 T}{\hat{\sigma}\sqrt{T}}. \\ D_2 &= D_1 - \hat{\sigma}\sqrt{T}. \end{aligned}$$

$C(F_{0,T}, K, T)^{model}$ and $P(F_{0,T}, K, T)^{model}$ are the model's European calls and puts, r the risk-free rate, $\hat{\sigma}$ the interpolated/extrapolated volatility given by the model in Equation (30) and $\Phi(\cdot)$ is the standard normal cumulative function.

By this methodology, we obtain a continuous value of the Equations (8) and (12),

$$\begin{aligned}\mathbb{E}_0^{\mathbb{Q}}\left[e^{-rT}RP_T\right]^{model} &= 2\int_0^{F_{0,T}} \frac{1}{K^2}P(F_{0,T},K,T)^{model}dK \\ &+ 2\int_{F_{0,T}}^{\infty} \frac{1}{K^2}C(F_{0,T},K,T)^{model}dK.\end{aligned} \tag{31}$$

$$\mathbb{RIX}^{model} = 2\left\{\int_0^{F_{0,T}} \frac{\ln(\frac{F_{0,T}}{K})}{K^2}P(F_{0,T},K,T)^{model}\,dK\right\}, \tag{32}$$

where we apply the identical scaling transformation of Equation (21) to both equations.

This model proves to be relevant for evaluating our contracts for several reasons. Firstly, it provides access to a daily continuous volatility surface. Additionally, it ensures coherence with the risk-neutral measure. The model successfully captures stylized facts, including the smile attenuation and smirk of the S&P 500. Its simplicity of interpretation and computation further enhances its relevance for practitioners.

Another crucial aspect to consider for an asset pricing model is its consistency with the absence of arbitrage assumption. François et al. (2022) [22] demonstrate the coherence of the pricing generated by the model with a limited static arbitrage opportunities. The demonstration draws inspiration from the work of Davis and Hobson (2007) [17], involving the construction of a spread portfolio. The key motivation behind considering this model for our paper is its robustness in handling a continuum of options across various strikes. With these results, the continuous valuation of $\mathbb{E}_0^{\mathbb{Q}}\left[e^{-rT}RP_T\right]$ becomes straightforward.

4.3 Results of valuation

In this subsection, we present the findings of the evaluation of the two contracts. Initially, we delve into the assessment of the variance contract, followed by the subsequent examination of the $\mathbb{RIX}$. The valuation of each contract is conducted with a 30-day horizon, and we provide a brief statistical comparison of the two valuation methods for each contract.

4.3.1 Valuation of the variance contract

Despite the valuation methods of 4.1 and 4.2, another issue arises like in Section 3.3.1. The concern lies in the selection of available contracts, particularly calls at each rolling date. Indeed, this problem was also our issue for the replication of RP_T in Section 3.3. Specifically, there is a shortage of available call contracts, especially in the earliest years of our sample. Note that the proposed parametric model is not subject to this issue, as it is calibrated daily. Through interpolation or extrapolation, any contract can be evaluated for any business day in alignment with the risk-neutral volatility surface at time t.

For the 30-day contracts, we consider all the inception dates obtained in Section 3.3.1. This selection is due only to the comparative purpose of the two models. Only the trapezoidal method is restricted by quoted options dates standardization.

To evaluate the spread of the two methods, we suggest the relative metric: $PS_t = \frac{P_{m,t} - P_{d,t}}{P_{d,t}}$. P_t^m and P_t^d are respectively the value of the variance contract from the model and the trapezoidal rule at initiation $t_0 = 0$.

Table 16: Descriptive statistics of PS_t on a 30 days variance contract

Min.	1st Qu.	Median	Mean	3rd Qu.	Max.	SD
-8.517%	2.294%	6.247%	8.097%	11.555%	47.589%	8.4084%

Descriptive statistics of PS_t for the variance contract. The metrics are respectively the minimum (Min), maximum (Max), first quantile (1st Qu.), third quantile (3rd Qu.), and standard deviation (SD).

Figure 15: Variance contract Valuation by Methods

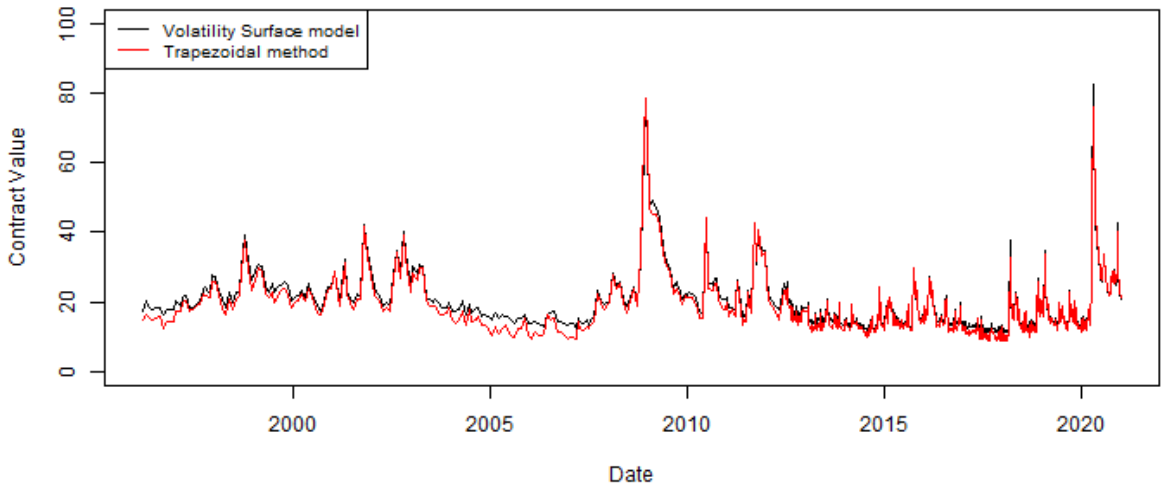

Comparative time series of the evaluation of the 30-day variance contract, with the trapezoidal method estimated by scaled Equation (27) and the volatility surface method estimated by scaled Equation (31). The inception dates t_0 align with those in Section 3.3.

According to the findings presented in Table 16, the metrics suggest a low spread on average, indicating an reasonable fit of the model. Figure 15 illustrates that both models effectively capture various spikes linked to different financial turmoils. However, a notable difference arises as the implied volatility (IV) parametric model tends to slightly overestimate the variance contract compared to the trapezoidal model, particularly in periods of low volatility before the 2007-2008 financial crisis.

To investigate this discrepancy, we leverage the empirical findings from the regression analysis in Section 3.3.4 by comparing the minimum and maximum moneyness of the two methods for the one-month variance contract. Figure 16 illustrates insights we can draw regarding the spread of the two valuation methods. The model's ability to extrapolate/interpolate options prices provides a lower truncation error by offering a larger range of the strike price grid. The combination of a lower K^{min} and greater K^{max} results in a higher value for the options portfolio, as explained in Section 3.3.4.

Additionally, we observe a greater divergence for K^{max}, primarily attributed to a larger proportion of puts than calls in our real data sample. There is also a convergence concerning K^{min} during both the financial crisis of 2008 and the COVID-19 crisis.

Figure 16: Comparative time series of the moneyness between the two valuation method

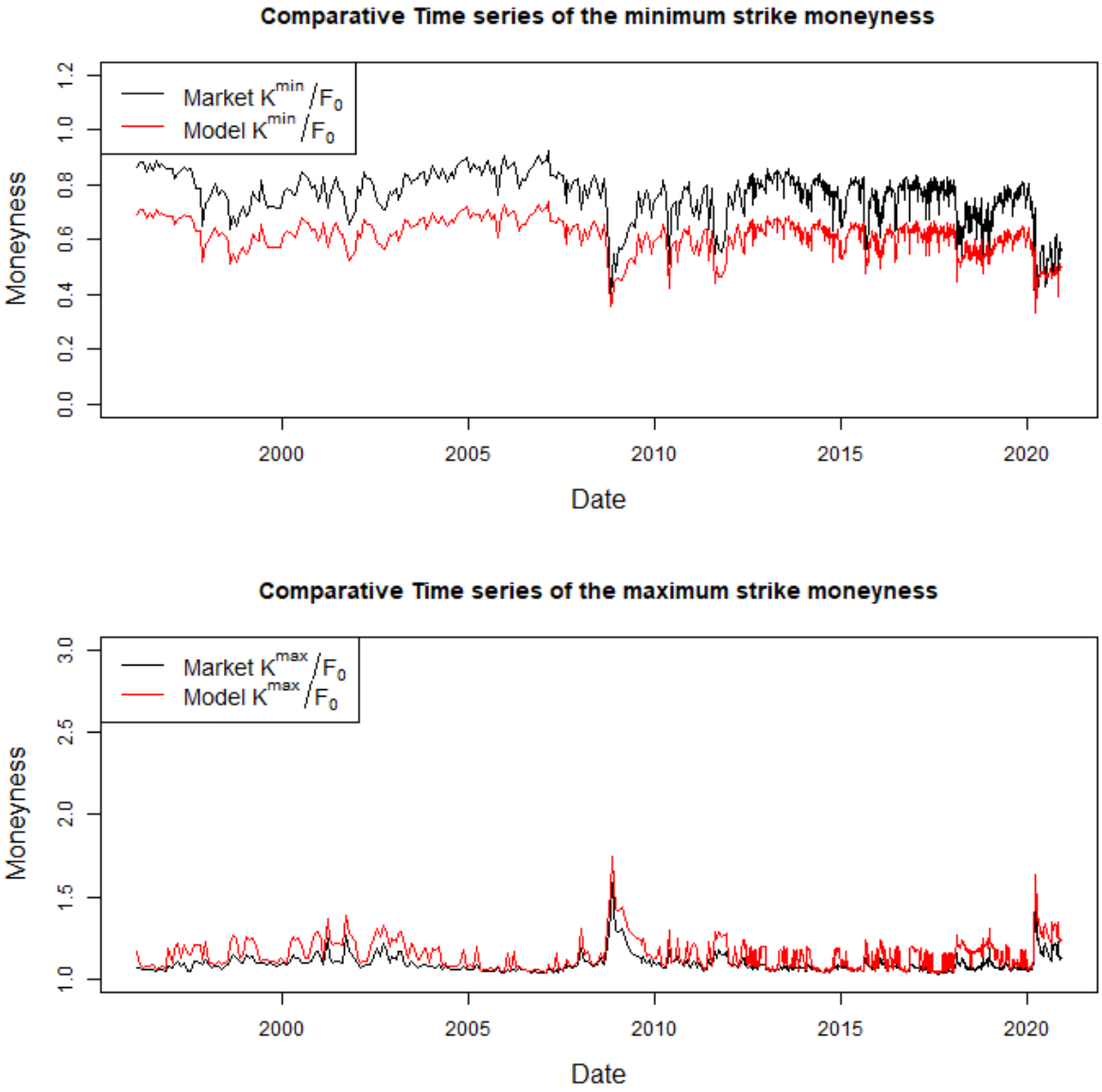

Comparative time series of the moneyness for the minimum K^{min} and maximum K^{max} strikes, calculated for the two valuation methods by dividing them by the initial future prices $F_{0,T}$.

4.3.2 Valuation of the $\mathbb{RIX}$

In this section, we employ the two methodologies outlined in Section 4.1 to evaluate $\mathbb{RIX}$ contract at $t_0 = 0$. We conduct a comparative analysis similar to that carried out for the variance contract in the preceding subsection, 4.3.1.

Table 17: Descriptive statistics of PS_t on a 30 days $\mathbb{RIX}$

Min.	1st Qu.	Median	Mean	3rd Qu.	Max.	SD
-8.851%	21.154 %	43.899%	56.008%	77.674%	345.825%	49.4845%

Descriptive statistics for RIX valuation using the PS_t metric. The other metrics are respectively the minimum (Min), maximum (Max), first quantile (1st Qu.), third quantile (3rd Qu.), and standard deviation (SD).

Figure 17: $\mathbb{RIX}$ Valuation by Methods

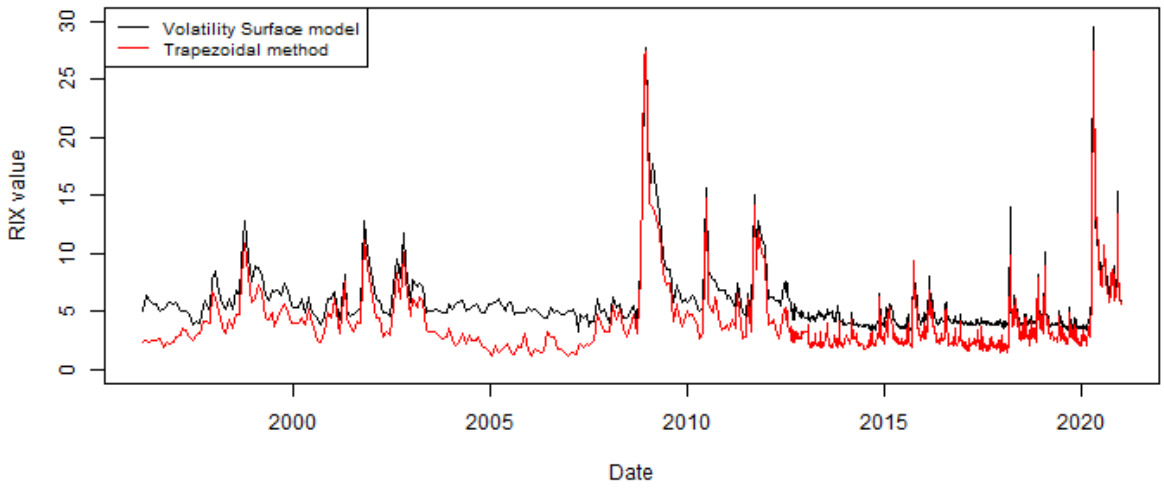

Comparative time series of the evaluation of the $\mathbb{RIX}$, with the trapezoidal method estimated by Equation (28) and the volatility surface method estimated by Equation (32). The inception dates t_0 align with those in Section 3.3.

As observed in Table 17, the spread is higher for the $\mathbb{RIX}$ compared to our other contract. This difference primarily stems from the construction of the $\mathbb{RIX}$. Referring to Equation (12), the index is formed based on a specific portfolio of options, which contrasts with the one outlined in Equation (8). Unlike the variance contract, the $\mathbb{RIX}$ aims to capture only extreme negative returns by considering exclusively out-of-the-money puts, with a greater emphasis on deep out-of-the-money puts. In other words, the $\mathbb{RIX}$ portfolio assigns weights based on the moneyness level: the deeper out-of-the-money the put, the larger the assigned weight. Consequently, as observed in Figure 16, the volatility surface model provides a broader range of deep out-of-the-money puts moneyness, directly influencing the construction of the $\mathbb{RIX}$ portfolio. As illustrated in Figure 17, during higher volatility periods, the two methods align in evaluating negative extreme events. However, the contrast becomes evident during calmer periods.

5 Conclusion

In our research paper, we delve into the challenges associated with the replication and mark-to-market valuation of a derivative product contingent on the quadratic variation of the S&P 500. The replication consists of two components: a continuous options portfolio comprising out-of-the-money European calls and puts options, and a dynamic strategy involving daily rebalancing on the futures contract.

The contract replication is primarily assessed in a simulated environment for a 30-day horizon by discretizing the option portfolio using the trapezoidal method. The simulation results highlight two main potential sources of replication errors, both centered around the static part: the distance between the strike prices and the truncation error.

Secondly, we replicate the contract using real futures and options data, with a sample spanning from January 1996 to December 2020. Our replication strategy is evaluated over four different time horizons: one month, three months, six months, and one year. In the data study, the strategies generally perform well. However, significant errors are identified on certain trading days. We conduct a regression analysis on the replication's relative errors to identify potential sources of these discrepancies. Our analysis reveals that these variations are attributed to two key factors. Firstly, there is an error in truncation concerning the limits of the numerical integral used to evaluate the static options portfolio. Secondly, there is an enhanced replication performance during crisis periods, characterized by a combination of negative shocks to the underlying asset and an increase in monthly implied volatility for at-the-money options.

In Section 4, we observe similar results for the valuation of the contract at the inception date. Consequently, we introduce a parametric model, based on the findings of François et al. (2022) [22], which facilitates continuous replication of the static portfolio, allowing for a comparison with the non-parametric trapezoidal method. Our comparative analysis focuses on 30-day contracts. The parametric model performs well in capturing both low and high-volatility periods. Notably, in the earliest part of our sample, the model tends to overestimate the variance contract, primarily due to its ability to reduce the truncation error by producing a wider range of strike prices.

After conducting our testing, we extend the comparison to the $\mathbb{RIX}$. Interestingly, our findings for this contract differ. Given its focus on negative extreme events, the $\mathbb{RIX}$ portfolio comprises only out-of-the-money (OTM) puts, assigning larger weights as the moneyness of these OTM puts decreases. Our results indicate that both valuation methods can effectively capture these extreme negative events. However, during low volatility periods, a noticeable disparity emerges. As the implied volatility (IV) parametric model can generate a wider range of strikes, the weights of the $\mathbb{RIX}$ portfolio are even more affected since they are also a function of the moneyness of deeper out-of-the-money (OTM) puts. Consequently, the model tends to overestimate the $\mathbb{RIX}$ index in these calmer periods.

Finally, we highlight the potential for future research to explore the replication and valuation of similar derivatives, considering other risk-neutral moments. While our current study focuses on the S&P 500 index, there is significant interest in extending these methodologies to individual stocks, sector-specific exchange-traded funds, and commodities.

6 References

References

[1] Andersen, T. G., Bondarenko,O., Todorov V., and Tauchen,G.(2015), The fine structure of equity-index option dynamics. *Journal of Econometrics*,187:532–546.

[2] Bakshi, G.,Kapadia, N. and Madan,D. (2003), Stock Return Characteristics, Skew Laws, and the Differential Pricing of Individual Equity Options. *The Review of Financial Studies*,16(1).

[3] Bates,D.S(1996), Jumps and Stochastic volatility: Exchange Rate Processes Implicity in Deutsche Mark Options. *The Review of Financial Studies*, 9(1):69-107.

[4] Begin.J.F and Gauthier.G(2020), Price bias and common practice in option pricing. *The Canadian Journal of Statistics*, 48:8–35.

[5] Black,F., Scholes,M(1973), The pricing of options and corporate liabilities. *Journal of Political Economy*, 81:637-654.

[6] Bondarenko,O (2014), Variance trading and market price of variance risk. *Journal of Econometrics*, 180: 81-97.

[7] Boyle.P.P and Emanuel.D(1980), Discretely Adjusted Option Hedges. *Journal of Financial Economics*, 8: 259-282.

[8] Britten-Jones, M., Neuberger, A(2000), Option prices, implied price processes, and stochastic volatility. *Journal of Finance*, 55 (2): 839-866.

[9] Chalamandaris, G. and Tsekrekos, A. E. (2011), How important is the term structure in implied volatility surface modeling? Evidence from foreign exchange options. *Journal of International Money and Finance,* 30(4):623–640.

[10] Carr,P.,Geman,H.,Madan,D. and Yor.M (2002), The finite structure of asset returns: an empirical investigation. *The Journal of Business*, 75(2):305-332

[11] Carr,P. and Madan,D. (1998), Towards a Theory of Volatility Trading

[12] Carr, P. and Lee, R.(2007), Realized volatility and variance: options via swaps. *Risk*, May 2007:76:83.

[13] Carr, P. and Wu, L.(2002), Static Hedging of Standard Options. *NYU Tandon Research Paper*, No 585451.

[14] Carr, P. and Wu, L.(2009), Variance risk premiums. *Review of Financial Studies*. 22:1311-1341

[15] Cboe website, CBOE VIX White paper.

[16] Cvitanic, J. and Karatzas, I.(1999), On dynamic measures of risk. *Finance and Stochastics* , 3:451-482

[17] Davis, M. and Hobson, D.(2007), The range of traded options. *Mathematical finance* , 17(1):1-14

[18] Demeterfi, K., Derman, E., Kamal, M., Zou, J(1999), A guide to volatility and variance swaps. *Journal of Derivatives*, 6(4):9-32.

[19] Derman.E and Taleb.N(2005), The illusions of dynamic replication. *Quantitative Finance*, 5(4):323-326.

[20] Dewynne,J.N and Putyatin.E(1999), Market liquidity and its effect on option valuation and hedging.*The Royal Society*, 357(1758):2093-2108.

[21] Du.J and Kapadia,N.(2012), Tail and Volatility Indices from Option Prices.

[22] Francois,P., Galarneau-Vincent,R., Gauthier,G. and Godin.F(2022), Venturing into Uncharted Territory: An Extensible Parametric Implied Volatility Surface Model. *Journal of Futures Markets*, 42(10):1912-1940

[23] Francois,P., Gauthier,G. and Godin.F(2014), Optimal hedging when the underlying asset follows a regime-switching Markov process. *European Journal of Operational Research*, 237(1):312-322.

[24] Gao,G.P ,Gao.P, and Song.Z(2018), Do hedge funds exploit rare disaster concerns?. *The Review of Financial Studies*, 31:2650-2692.

[25] Gauthier, G. and Simonato, J.-G. (2012), Linearized Nelson-Siegel and Svensson models for the estimation of spot interest rates. *European Journal of Operational Research,* 219(2):442–451.

[26] Goncalves, S. and Guidolin, M.(2006), Predictable dynamics in the S&P 500 index options implied volatility surface. *Journal of Business*, 79(3):1591–1635.

[27] Hull,J.(2018), Options, Futures, and Other Derivatives. *9th Global Ed.,Pearson*,p.267-269

[28] Hull,J and White.A (2017), Optimal Delta Hedging. *Journal of Banking and Finance*, 82: 180-190.

[29] Hurn,A.S. ,Lindsay,K.A. and McClelland,A.J.(2015), Estimating the Parameters of Stochastic Volatility Models Using Option Price Data. *Journal of Business and Economic Statistics*, 33(4):579-594.

[30] Kahneman.D and Tversky.A(1979), Prospect Theory: An Analysis of Decision under Risk. *Econometrica*, 47(2):263-292.

[31] Mandelbrot.B(1963), The Variation of Certain Speculative Prices. *Journal of Business*, 36(4):394-419.

[32] Mandelbrot.B(1997), Fractals and Scaling in Finance. *Springer Selecta Volume E*

[33] Psychoyios.D and Skiadopoulos.G(2005),
Volatility options: Hedging effectiveness,pricing and model error. *Journal of Futures Markets*, 26: 1-31.

[34] Remillard.B and Rubenthaler.S(2009), Optimal hedging in discrete and continuous time. *Technical Report-GERAD*,G-2009-77.

[35] Sekine.J (2004), Dynamic minimization of worst conditional expectation of shortfall. *Mathematical Finance*,14,605-618

[36] Taleb.N (2009), Errors, robustness, and the fourth quadrant. *International Journal of Forecasting*, 25(4),744-759

[37] Xu.M (2006), Risk measure pricing and hedging in incomplete markets. *Annals of Finance volume*, 2:51-71

A $\mathbb{RIX}$ derivations

First, the risk-neutral variance of the log returns is

$$\mathbb{E}_0^{\mathbb{Q}}\left[\left(\ln\left(\frac{F_{t,T}}{F_{0,T}}\right)-\mathbb{E}_0^{\mathbb{Q}}\left[\ln\left(\frac{F_{t,T}}{F_{0,T}}\right)\right]\right)^2\right]=\mathrm{Var}_0^{\mathbb{Q}}\left(\ln\frac{F_{t,T}}{F_{0,T}}\right).$$

To build the intuition, we take into consideration the payoff $g(F_{t,T})=\left(\ln\frac{F_{t,T}}{F_{0,T}}\right)^2$. Applying the Itô's lemma, we obtain

$$\begin{aligned}\left(\ln\frac{F_{t,T}}{F_{0,T}}\right)^2=&\int_{0^+}^{t}\frac{2}{F_{u^-,T}}\left(\ln\frac{F_{u^-,T}}{F_{0,T}}\right)dF_{u,T}+\int_{0^+}^{t}\left(1-\ln\frac{F_{u^-,T}}{F_{0,T}}\right)V_{u^-}du\\&+\sum_{0^+<u<t}\left\{\ln\left(\frac{F_{u,T}}{F_{0,T}}\right)^2-\ln\left(\frac{F_{u^-,T}}{F_{0,T}}\right)^2-\frac{2}{F_{u^-,T}}\left(\ln\frac{F_{u^-,T}}{F_{0,T}}\right)\Delta F_u\right\}.\end{aligned}\tag{33}$$

We apply the Carr-Madan formula (1998) for the payoff $\left(\ln\frac{F_{t,T}}{F_{0,T}}\right)^2$,

$$\begin{aligned}\left(\ln\frac{F_{t,T}}{F_{0,T}}\right)^2=&\left(\ln\frac{F_{0,T}}{F_{0,T}}\right)^2+\frac{2}{F_{t,T}}\left(\ln\frac{F_{0,T}}{F_{0,T}}\right)(F_{t,T}-F_{0,T})\\&+2\left\{\int_0^{F_{0,T}}\frac{1-\ln\left(\frac{K}{F_{0,T}}\right)}{K^2}(K-F_{t,T})^+\,dK+\int_{F_{0,T}}^{\infty}\frac{1-\ln\left(\frac{K}{F_{0,T}}\right)}{K^2}(F_{t,T}-K)^+\,dK\right\}.\end{aligned}$$

With simplifications, we retrieve the discounted expression of the payoff[12]

$$\begin{aligned}\mathbb{E}_0^{\mathbb{Q}}\left[e^{-rT}\ln\left(\frac{F_{t,T}}{F_{0,T}}\right)^2\right]\cong 2&\left\{\int_0^{F_{0,T}}\frac{1+\ln\left(\frac{F_{0,T}}{K}\right)}{K^2}P(F_{0,T},K,T)\,dK\right.\\&\left.+\int_{F_{0,T}}^{\infty}\frac{1-\ln\left(\frac{K}{F_{0,T}}\right)}{K^2}C(F_{0,T},K,T)\,dK\right\}.\end{aligned}\tag{34}$$

[12]The method for obtaining a detailed computation of these results is outlined in the study conducted by Bakshi, Kapadia, and Madan (2003) [2].

Moving ahead with constructing $\mathbb{RIX}$, we merge the equality of integrated variance and the jump terms from Equation (3) with the replication results from Carr Madan in Equation (6). This combination leads to the conclusion that

$$\begin{aligned}
&\int_{0^+}^{t} V_{u^-}du + \sum_{0^+<u<t} \frac{1}{2}\xi^2_{u^-}(\Delta J_u)^2 \\
&\cong 2\left\{\int_0^{F_{0,T}} \frac{1}{K^2}(K-F_{t,T})^+dK + \int_{F_{0,T}}^{\infty} \frac{1}{K^2}(F_{t,T}-K)^+dK\right\} \\
&+ 2\sum_{i=1}^{n}\left(\frac{1}{F_{t_{i-1},T}} - \frac{1}{F_{0,T}}\right)(F_{t_i,T} - F_{t_{i-1},T}).
\end{aligned} \tag{35}$$

Multiplying both sides of Equation (35) by the discount factor and taking the risk-neutral expectation,

$$\begin{aligned}
&\mathbb{E}_0^{\mathbb{Q}}\left[e^{-rT}\left(\int_{0^+}^{t} V_{u^-}du + \sum_{0^+<u<t} \frac{1}{2}\xi^2_{u^-}(\Delta J_u)^2\right)\right] \\
&\cong 2\left\{\int_0^{F_{0,T}} \frac{1}{K^2}P(F_{0,T},K,T)dK + \int_{F_{0,T}}^{\infty} \frac{1}{K^2}C(F_{0,T},K,T)dK\right\},
\end{aligned} \tag{36}$$

similarly to the derivation in Section 2.4.1, the risk-neutral expectation of the dynamic strategy is $\mathbb{E}_0^{\mathbb{Q}}\left[2\sum_{i=1}^{n}\left(\frac{1}{F_{t_{i-1},T}} - \frac{1}{F_{0,T}}\right)(F_{t_i,T} - F_{t_{i-1},T})\right] = 0$.

We then connect the risk-neutral expectation of this spread to the construction of the $\mathbb{RIX}$ replicating portfolio. By the use of the result of Equation (36), we apply a spread of the risk-neutral expectations: $\mathbb{E}_0^{\mathbb{Q}}\left[e^{-rT}\ln\left(\frac{F_{t,T}}{F_{0,T}}\right)^2\right] - \mathbb{E}_0^{\mathbb{Q}}\left[e^{-rT}\ln\left(\frac{F_{t,T}}{F_{0,T}}\right)\right]$.

By the results of Equations (34) and (36),

$$\begin{aligned}
\Pi_t^1 &= 2\left\{\int_0^{F_{0,T}} \frac{1+\ln\left(\frac{F_{0,T}}{K}\right)}{K^2}P(F_{0,T},K,T)\,dK + \int_{F_{0,T}}^{\infty} \frac{1-\ln\left(\frac{K}{F_{0,T}}\right)}{K^2}C(F_{0,T},K,T)\,dK\right\}. \\
\Pi_t^2 &= 2\left\{\int_0^{F_{0,T}} \frac{1}{K^2}P(F_{0,T},K,T)\,dK + \int_{F_{0,T}}^{\infty} \frac{1}{K^2}C(F_{0,T},K,T)\,dK\right\}.
\end{aligned}$$

which leads to

$$\begin{aligned}
\Pi_t^1 - \Pi_t^2 = 2\Bigg\{&\int_0^{F_{0,T}} \frac{\ln\left(\frac{F_{0,T}}{K}\right)}{K^2}P(F_{0,T},K,T)\,dK \\
&- \int_{F_{0,T}}^{\infty} \frac{\ln\left(\frac{K}{F_{0,T}}\right)}{K^2}C(F_{0,T},K,T)\,dK\Bigg\}.
\end{aligned} \tag{37}$$

To gain additional insight, let's analyze the weights outlined in Equation (37). In the first part, as the strike price decreases, puts shift further out-of-the-money (OTM), resulting in larger weights for these puts. This implies an anticipation of a greater payoff for puts in the event of a negative jump. Similarly, in the second part, as the strike price increases, calls become more OTM, leading to higher weights for these calls and suggesting an increased expected payoff for them. From a risk management perspective, the objective is to guard against significant negative jumps. In this context, the section exclusively involving puts becomes especially relevant.

In contrast to Section 2.4.1, the idea of this portfolio spread is purely from a static replication perspective. In terms of the portfolio's notation, $\Pi_t^1 = \mathbb{E}_0^{\mathbb{Q}}\left[e^{-rT}\ln\left(\frac{F_{t,T}}{F_{0,T}}\right)^2\right]$ and $\Pi_t^2 = \mathbb{E}_0^{\mathbb{Q}}\left[e^{-rT}\ln\left(\frac{F_{t,T}}{F_{0,T}}\right)\right]$.

By the results obtained in Equation (37) we retrieve the jump tail index $\widehat{JTIX}$ found in Du and Kapadia (2012) [21]. Following Gao et al. (2018) [24], we construct the $\mathbb{RIX}$ (i.e., $\widehat{JTIX^-}$ in Du and Kapadia (2012) [21]). We consider only the downside of the Equation (37), with negative indicator $^-$ specifying that only puts are taken into account.

$$\mathbb{RIX} = \Pi_t^{1-} - \Pi_t^{2-}.$$

$$\mathbb{RIX} = 2\left\{\int_0^{F_{0,T}} \frac{\ln(\frac{F_{0,T}}{K})}{K^2} P(F_{0,T}, K, T)\, dK\right\}.$$

B Pseudo-Algorithm of the simulation

For further intuition, we provide in this subsection the pseudo-algorithm of the simulation. In the implementation, we consider the risk-neutral parameters given in Table 2: $\{\kappa, \theta, \sigma, \rho, \mu_{\xi_t}, \sigma_{\xi_t}, \lambda\}$. Additionally, we recall the discrete model of Subsection 3.2.1 and the Equations of Subsection 3.2.3.

For each future path, Bondarenko's quadratic variation is generated for n days. With those settings, we can compute Bqv_T and RP_T by obtaining the terminal 30-day future price.

We refer to the following pseudo-code for the implementation of 100 000 paths j,

1: **for** j `in 1:100 000` **do** ▷ Initialization of the paths simulations
2: $\Delta t \leftarrow T/n$ ▷ Setting the time step with maturity T and day step n
3: **for** t `in 1:n` **do** ▷ Initialization of the 30 days future trajectory
4: $V_{t+\Delta} \leftarrow V_t + \kappa(\theta - V_t^+)\Delta t + \sigma\sqrt{V_t^+}\sqrt{\Delta t}Z_{Cholesky}$ ▷ Volatility process
5: $Y_{t+\Delta} \leftarrow Y_t + \left(r - \frac{1}{2}V_t^+ - e^{\mu_{\xi_{t^-}} + \frac{1}{2}\sigma^2_{\xi_{t^-}}}\lambda\right)\Delta t + \sqrt{V_t^+\Delta t}Z_1 + \sum_{i=1}^{J} Z_i$ ▷ Log-stock
6: $F_{t+\Delta t,T} \leftarrow \exp\left(Y_{t+\Delta,T}\ e^{r\Delta t}\right)$ ▷ Computation of the future
7: $DS_t^j \leftarrow$ `Equation(18)` ▷ Computation of the dynamical position at t
8: **end for** ▷ End of the Future trajectory loop
9: $Bqv_T^j \leftarrow$ `Equation(16)` ▷ Computation of the observed Bqv
10: $OP_t^j \leftarrow$ `Equation(17)` ▷ Computation of options portfolio terminal payoff
11: $RP_T^j \leftarrow$ `Equation(19)` ▷ Sum of lines (7) and (11) to obtain the replication
12: $sBqv_T^j \leftarrow$ `Equation(20)` ▷ Scaled transformation of the observed Bqv
13: $sRP_T^j \leftarrow$ `Equation(21)` ▷ Scaled transformation for the replication portfolio
14: $e^j \leftarrow$ `Equation(22)` ▷ Computation of the Replication Error by lines (13)-(12)
15: $\epsilon^j \leftarrow$ `Equation(23)` ▷ Computation of the relative error
16: **end for**
17: RRMSE $\leftarrow$ `Equation(24)` ▷ Computation of RRMSE for the whole simulation

Note that $Z_{Cholesky}$ is the Brownian decomposition as defined in 3.1. In addition, for each ΔK_i case the difference is the weights $\frac{1}{K^2}$ of the options terminal payoff we obtain in line 10.

C Regression analysis

C.1 Correlation Matrix

The following tables display the correlation matrix for each replicating strategy concerning the various variables selected in the regressions of Section 3.3.4.

Our first concern is with the relative error ϵ in relation to the other variables. This information is presented in the first columns of Tables 18 to 21.

Since the relative error ϵ is defined as $\epsilon = \frac{(sRP_T - SBqv_T)}{SBqv_T}$, a negative correlation would imply under-replication, and a positive correlation would indicate over-replication. We observe that the sign of the correlation between the sets of explanatory variables and ϵ is identical.

Firstly, the number of contracts is positively correlated, indicating over-performance when this variable increases. Secondly, the minimum moneyness $\frac{K^{min}}{F_{0,T}}$ is negatively correlated, suggesting that an increase in the minimum strike will elevate the truncation error of the integrals of OP_T and cause under-performance of the strategies. Regarding the maximum moneyness $\frac{K^{max}}{F_{0,T}}$, there is a positive correlation with ϵ, indicating over-performance of the strategies when the maximum strike increases. As for the at-the-money 30-day implied volatility, the correlation is positive, signifying over-performance of the replication when there is a volatility spike. Analogously, with these variables, the log return is negatively correlated, suggesting that in the case of positive (negative) jumps, the replication is under (over) performing.

The remaining correlations between the variables indicate an absence of multicollinearity that could bias our regression estimation.

Table 18: Correlation Matrix for the one-month rollover

	ϵ	Number of contracts	$\frac{K^{min}}{F_{0,T}}$	$\frac{K^{max}}{F_{0,T}}$	30-day ATM IV	$\ln\left(\frac{F_{t,T}}{F_{0,T}}\right)$
ϵ	1					
Number of contracts	0.1375	1				
$\frac{K^{min}}{F_{0,T}}$	-0.1830	-0.5320	1			
$\frac{K^{max}}{F_{0,T}}$	0.1362	0.2404	-0.6808	1		
30-day ATM IV	0.1615	0.1059	-0.4576	0.6152	1	
$\ln\left(\frac{F_{t,T}}{F_{0,T}}\right)$	-0.1949	0.0359	-0.0687	0.1696	-0.4224	1

Correlation matrix for the one-month replication strategies with the relative error ϵ, the number of contracts, the minimum and maximum moneyness, the at-the-money 30-day implied volatility, and the log return on the contract duration (from t_0 to T).

Table 19: Correlation Matrix for the three-month rollover

	ϵ	Number of contracts	$\frac{K^{min}}{F_{0,T}}$	$\frac{K^{max}}{F_{0,T}}$	30-day ATM IV	$\ln\left(\frac{F_{t,T}}{F_{0,T}}\right)$
ϵ	1					
Number of contracts	0.1471	1				
$\frac{K^{min}}{F_{0,T}}$	-0.1493	-0.5231	1			
$\frac{K^{max}}{F_{0,T}}$	0.1263	0.1914	-0.5862	1		
30-day ATM IV	0.0321	-0.0796	-0.0814	0.4200	1	
$\ln\left(\frac{F_{t,T}}{F_{0,T}}\right)$	-0.2189	0.0830	-0.2083	0.2653	-0.4572	1

Correlation matrix for the three-month replication strategies with the relative error ϵ, the number of contracts, the minimum and maximum moneyness, the at-the-money 30-day implied volatility, and the log return on the contract duration (from t_0 to T).

Table 20: Correlation Matrix for the six-month rollover

	ϵ	Number of contracts	$\frac{K^{min}}{F_{0,T}}$	$\frac{K^{max}}{F_{0,T}}$	30-day ATM IV	$\ln\left(\frac{F_{t,T}}{F_{0,T}}\right)$
ϵ	1					
Number of contracts	0.1180	1				
$\frac{K^{min}}{F_{0,T}}$	-0.0493	-0.4679	1			
$\frac{K^{max}}{F_{0,T}}$	0.0690	0.1099	-0.2459	1		
30-day ATM IV	0.0929	0.1231	0.1244	0.3968	1	
$\ln\left(\frac{F_{t,T}}{F_{0,T}}\right)$	-0.2244	0.0604	-0.3330	0.1266	-0.5897	1

Correlation matrix for the six-month replication strategies with the relative error ϵ, the number of contracts, the minimum and maximum moneyness, the at-the-money 30-day implied volatility, and the log return on the contract duration (from t_0 to T).

Table 21: Correlation Matrix for the one-year rollover

	ϵ	Number of contracts	$\frac{K^{min}}{F_{0,T}}$	$\frac{K^{max}}{F_{0,T}}$	30-day ATM IV	$\ln\left(\frac{F_{t,T}}{F_{0,T}}\right)$
ϵ	1					
Number of contracts	0.2211	1				
$\frac{K^{min}}{F_{0,T}}$	-0.0697	-0.4890	1			
$\frac{K^{max}}{F_{0,T}}$	0.2417	0.1654	-0.3138	1		
30-day ATM IV	0.0735	-0.0332	0.2452	0.0499	1	
$\ln\left(\frac{F_{t,T}}{F_{0,T}}\right)$	-0.2934	0.1949	-0.4600	0.1446	-0.5399	1

Correlation matrix for the one-year replication strategies with the relative error ϵ, the number of contracts, the minimum and maximum moneyness, the at-the-money 30-day implied volatility, and the log return on the contract duration (from t_0 to T).

D Volatility surface model

In François et al. (2022) [22], the parametric volatility surface model is a linear combination of risk factors. Therefore, this parametric model generates a daily implied volatility $\hat{\sigma}(M,T)$ for a given future's maturity (365-day basis) T and a moneyness M.

$$\hat{\sigma}(M,T) = \beta_1 + \beta_2 \exp\left(-\sqrt{T/T_c}\right) + \beta_3 \left(M \mathbb{1}_{M \geqq 0} + \frac{e^{2M}-1}{e^{2M}+1} \mathbb{1}_{M<0}\right) + \beta_4 \left(1 - \exp\left(-M^2\right)\right) \ln\left(T/T_m\right) + \beta_5 \left(1 - \exp\left((3M)^3\right)\right) \ln\left(T/T_m\right) \mathbb{1}_{M<0},$$

β_1 captures the long-term at-the-money implied volatility level, β_2 the time to maturity slope, β_3 the moneyness slope, β_4 the smile attenuation and β_5 the smirk. In addition, the model relates to two fixed values: T_m and T_c respectively a proxy of the sample's largest maturity and the location of the IV term structure's convexity change.

Following the estimation procedures in François et al. (2022) [22], the parameters are obtained using a minimization of the sum of squared errors in terms of implied volatility. The approach uses a Bayesian regularization to preserve the economic interpretation of the coefficients. The motivation of this Bayesian add-on is the existence of more than one set of parameters that fit the observed surface. The set of parameters for a sample's day τ, $\beta^{prior} = \{ATM_{1y,\tau}, Slope_\tau, \beta_{3,\tau-1}, \beta_{5,\tau-1}\}$ is clarified in Appendix D.2 .

Moneyness is defined as :

$$M = \frac{1}{\sqrt{T}} \ln\left(\frac{F_{t,T}}{K}\right). \tag{38}$$

Here T is the 365-day annualized time to maturity, $F_{t,T}$ the future price, and K is the strike price.

The data cleaning consists of the following filtration steps: removing the options quotes of short expiration dates (less than six days) and the quoted mid-price lower than 0.375$ (or zero bid) price. The following procedure is to exclude all the in-the-money options. The implied volatility of each mid-price option of the sample is computed by the usage of the Black formula (1976). The filtering results in an amount of 8,733,420 contracts over 6293 days.

Figure 18: Panel of the daily estimated parameter of the IV surface model

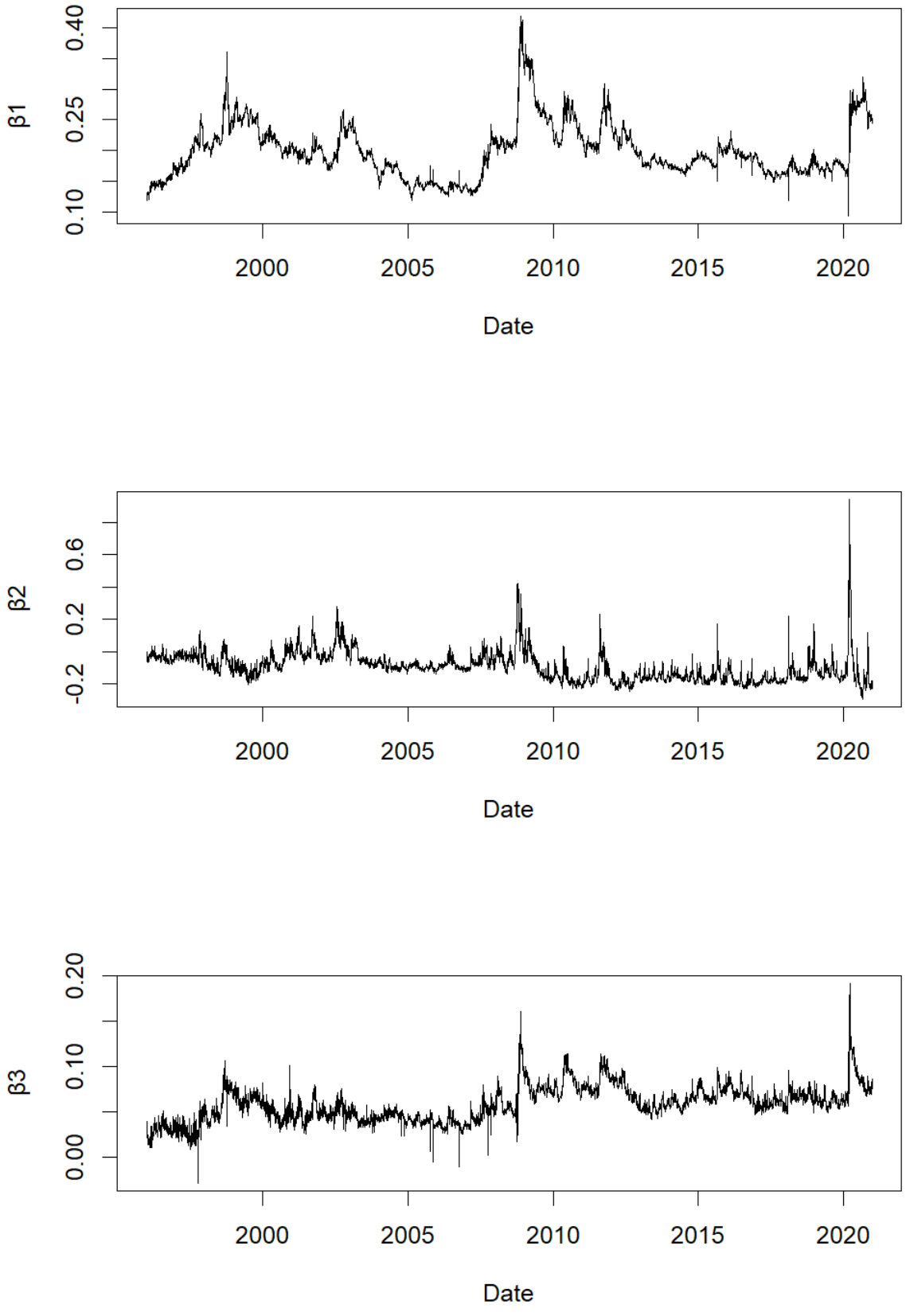

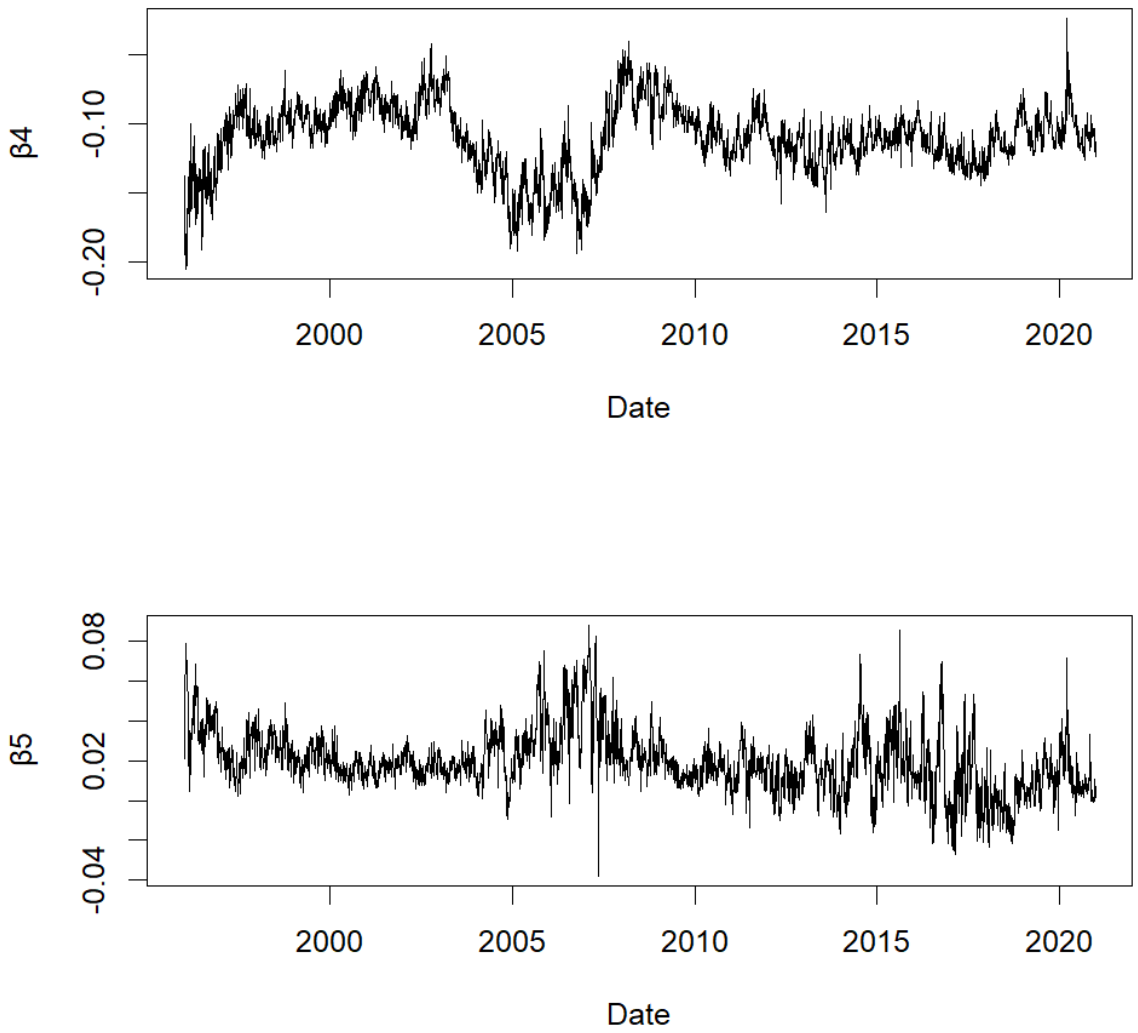

Panels of IV model's daily calibrated estimators for each sample's n day τ

Figure 18 above gives us many insights into the behavior of the component of the daily IV surface model. As demonstrated by François et al. (2022) [22], the level of the at-the-money IV is relatively low during normal market conditions and high during the financial crisis (1998 and 2008). The slope of the implied surface is most of the time positive, due to a positive β_2 parameter during periods of high volatility. This attenuation of the smile to be noisier during financial turmoil. The smile asymmetry captured by β_4 is more stable after the consecutive episode of the financial crisis (2008) and the flash crash of May 2010. And for β_5, the smirk seems to be more apparent in terms of level and volatility in more recent days.

D.1 RMSE of the model

For the sake of monitoring the quality of the in-sample fitting of our model, the daily root mean square error (RMSE) is therefore computed :

$$RMSE = \sqrt{\frac{1}{N}\sum_{n=1}^{N}(\sigma(M,T) - \sigma_T^o)^2}. \tag{39}$$

The model generates the price, denoted as $\sigma(M,T)$, for a specified moneyness (M) and maturity (T), while σ_T^o represents the observed implied volatility in the market. The daily time series is illustrated in Figure 19, and the descriptive statistics for the fitting Root Mean Square Error (RMSE) concerning moneyness and maturity are presented in Tables 22 and 23.

Figure 19: RMSE of the IV model on the volatility surface

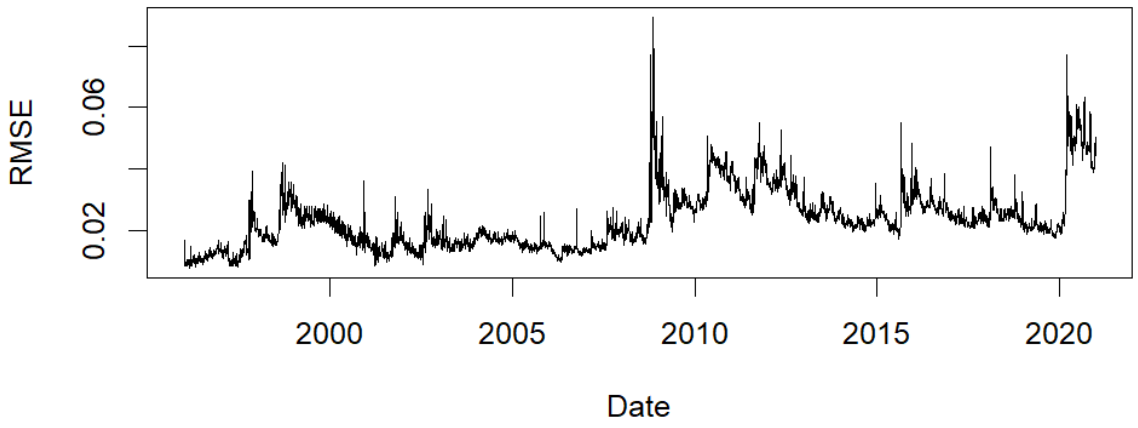

IV Model's RMSE during the period of 1996-01-03 to 2020-12-31

Table 22: Descriptive statistics of the RMSE S&P 500 options by moneyness

Moneyness	$M \leq -0.1$(call)	$-0.1 < M \leq 0.1$	$M > 0.1$(put)	All
Average RMSE	0.0174	0.0237	0.0252	0.0234
Number of contracts	1,490,728	2,054,803	5,187,889	8,733,420

Descriptive statistics of the daily S&P 500 options RMSE from January 4, 1996, to December 31, 2020, grouped by buckets of moneyness. M is the moneyness computed in Equation (38).

Table 23: Descriptive statistics of the RMSE S&P 500 options by maturity

Maturity	$T \leq 60$	$60 < T \leq 180$	$T > 180$	All
Average RMSE	0.0213	0.0179	0.0292	0.0234
Number of contracts	3,860,214	2,809,083	2,064,123	8,733,420

Descriptive statistics of the daily S&P 500 options RMSE from January 4, 1996, to December 31, 2020, grouped by buckets of moneyness. T is the annualized time to maturity on a 365-day basis.

The RMSE computation provides information on the fitting of the IV model. The average daily RMSE of the sample is 0.0234. The quality of the fitting deteriorates during extreme events. In terms of moneyness, Table 22 relates that the error of fitting is subject to a contrast between the types of options. The number of puts in the sample is greater than calls. The ARMSE (i.e. Average RMSE) for short and mid-term maturities is below the sample average, in contrast to long-term maturities where the ARMSE is higher than the average.

D.2 Bayesian extension

As an add-on the set of prior parameters is :

$$\beta^{prior} = \{ATM_{1y,\tau}, Slope_t, \beta_{3,\tau-1}, \beta_{5,\tau-1}\},$$

$ATM_{1y,\tau}$ is the observed one year at-the-money implied volatility. In our data, there is an issue for this measure due to the lack of traded one-year contracts at each market day. The proxy is to be selected for maturity between 260 and 370 days coupled with the smallest positive moneyness. This rule of thumb is applied according to the data available for each day. The same issue arises for the equivalent measure for one month $ATM_{1m,\tau}$. We apply a similar proxy for the same logistic reason. We selected maturities that are between 17 and 59 days coupled with the same criteria on the moneyness as previously mentioned (i.e., smallest positive).

From those approximations, we construct $Slope_\tau$

$$Slope_\tau = \frac{ATM_{1y,\tau} - ATM_{1m,\tau}}{\exp(-\sqrt{4/12})}$$

For the two other priors for $\beta_{3,\tau-1}$ and $\beta_{5,\tau-1}$ the previous day estimators are taken. No prior is attributed to β_4.

E Options trading strategies

The extensions of the straddle consist of the strip, the strap, and the strangle. Those three strategies are close to the straddle but offer flexibility in the order of the direction view of the trader. In the case of a strip, the position consists of buying one European call and two European puts, it allows a profit exposure if the large move is negative shock. Symmetrically a strap consists of two calls, and one put, it allows a profit if the large deviation is a positive shock. Another alternative is the strangle. This trading consists of one put and one call with the same expiration date but with a different strike. The call strike is higher than the put's strike. This strategy also allows a similar exposition to that of the straddle but requires a larger move of the underline. The details of the payoff of those strategies can be found in Hull p.268-269 [27]. Those strategies offer flexibility for the trader in terms of Greeks sensitivities and transaction costs.

Figure 20: Strip, strap and strangle

Figure 12.11 Profit from a strip and a strap.

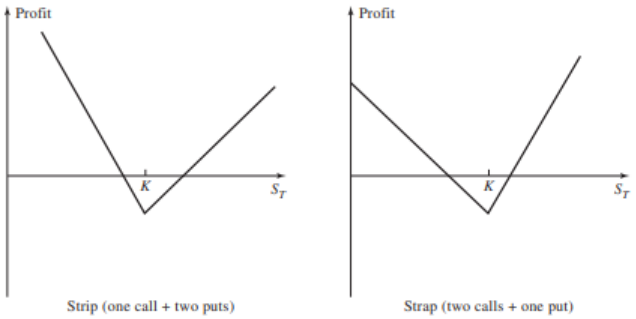

Figure 12.12 Profit from a strangle.

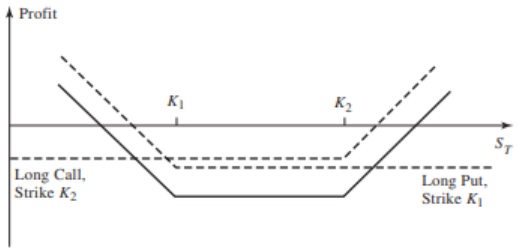

Table 12.6 Payoff from a strangle.

Range of stock price	*Payoff from call*	*Payoff from put*	*Total payoff*
$S_T \leqslant K_1$	0	$K_1 - S_T$	$K_1 - S_T$
$K_1 < S_T < K_2$	0	0	0
$S_T \geqslant K_2$	$S_T - K_2$	0	$S_T - K_2$

Figures 12.11 and 12.11 in Hull: Options, Futures, and Other Derivatives. 9th Global Edition, p.268-269[27].